CODEN:LUTEDX/(TEIE-5477)/1-078/(2022)

Industrial Electrical Engineering and Automation

Simulation of Transformer Inrush Currents and their Impact on the Grid

Juan de la Peña Toledo

Division of Industrial Electrical Engineering and Automation
Faculty of Engineering, Lund University

MSc Thesis
IEA Department at LTH

Popular Science Summary

Simulation of Transformer Inrush Currents and Their Impact on the Grid

Juan de la Peña Toledo

Abstract

When a transformer (an element with the ability to adapt voltage to the individual requirements of the different parts of the system) is switched in, a current inrush is drawn from the grid. The magnitude and duration of the inrush current depend on several factors, such as the size of the transformer and the network strength to which the transformer is being connected. To limit the disturbances that the energization of transformers may cause, their size is often constrained using a rule of thumb that relates the maximum transformer size to the network strength. This restriction comes from the fact that the larger the transformer is, the greater the inrush current and the deeper the voltage in the surrounding grid goes. This MSc Thesis aims to optimize the transformer sizing decision by precisely simulating the voltage dip at the energizing bus and the surrounding area. For this purpose, an adequate study of the causes and consequences of the inrush current phenomenon is conducted to design a Python model that can accurately represent these kinds of transient episodes. Afterwards, a steady-state software for power system analysis called PSS/E is used to estimate the impact on the surrounding area with limited fidelity. In conclusion, considering the limitations and assumptions made, it is possible to have some intuition on the expected impact of energizing a transformer in the grid in terms of the voltage dip in a more precise way than using the actual rule of thumb. However, some effort into verification is necessary.

Inrush currents during transformer energization are a well-known issue extensively described in the literature. Hence, modelling the equations that define its dynamics is a matter of understanding the different phenomena involved and making suitable assumptions. There are two types of transformers, but when it comes to the generation, transmission, distribution and industrial use of electrical power, three-phase transformers are dominant with respect to single-phase transformers. Still, because single-phase transformers are easier to comprehend, they are analysed first, and afterwards, the model is expanded to represent some classes of three-phase transformers. The result has excellent accuracy in comparison with other tools with superior transient analysis simulation such as Matlab Simscape or PSCAD. An example is available in Figure 1.

The next step is to find out the effect on the connected network, which relies on the PSS/E software because it is the main tool utilized at E.ON. The fact that is going to be used a steady-state program to estimate a transient effect is one of the challenges of this MSc Thesis and a limitation imposed by E.ON as they do not provide other software licenses.

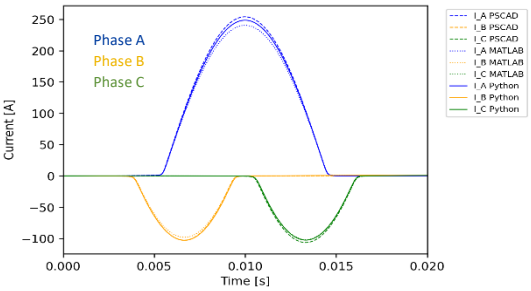

Figure 1: Inrush current waveform of a three-phase transformer compared to Matlab and PSCAD.

After developing different strategies to couple the time-simulation results with steady-state PSS/E variables and integrating everything in a Python tool, an energization study is carried out in a reduced grid. This allows us to evaluate the different alternatives and consider the most trustful ones, but the lack of measurements makes this task doubtful and non-verified.

Finally, with the information that E.ON engineers can extract from the tool designed for energization studies, it is possible to have an intuition about the voltage dip at different buses in the grid and make a transformer sizing decision given some boundary conditions imposed by grid standards or special customer requirements. Figure 2 shows the minimum voltage simulated at different buses when varying the size of the transformer being energized.

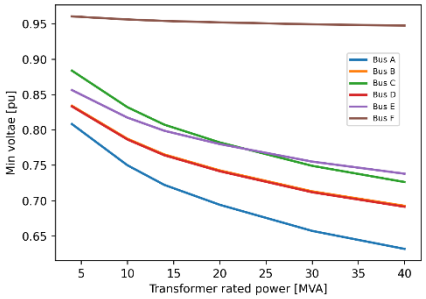

Figure 2: Simulated voltage dip at different buses

MSc Thesis

Simulation of Transformer Inrush Currents and their Impact on the Grid

Juan de la Peña Toledo
juan.delapenatoledo@gmail.com

June 30, 2022

Main supervisor: Olof Samuelsson
Assistant supervisor: Imran Maqbool
Company supervisor: Omar Juárez Moreno

LUNDS UNIVERSITET

Acknowledgements

I want to thank the professors Olof, Imran and Jörgen for their guidance, Lund University for receiving me during my last year of studies, all the new friends for creating unforgettable moments in Sweden and my family for making it possible. Special gratitude to Omar for trusting me in this project and advising me at any time.

I take this opportunity to promote the community involved in the open-source software used in this project: LaTeX, Python and its libraries (Tkinter, Matplotlib, Math, Numpy, Scipy, Pandas), diagrams.net, Github, Anaconda and Spyder.

Abstract

This MSc Thesis's main objective is to determine the impact of transformer inrush currents in the grid and develop a tool that helps E.ON Energidistribution AB evaluate transformer sizing. The motivation of E.ON is to have a more precise way to estimate the energization consequences of increasing the transformer size in the grid, since currently is being used a rule of thumb that relates the transformer rated power to the short-circuit capacity of the bus at which the transformer is connected. This rule of thumb is established because they have the concern that large power transformers can cause serious inrush currents.

An adequate study of the causes and consequences of the inrush current phenomenon is conducted to determine the duration and magnitude of undesired disturbances. Python is used to design simplified transformer models based on banks of three single-phase units due to substantial limitations of more advanced alternatives. PSCAD and Matlab Simscape Electrical, two superior transient analysis software, are used to verify the results of test simulations. The non-linearity of the differential system of equations required numerical methods and the utilization of the Trapezoidal Rule of Integration and the Newton Raphson Method.

Then, different strategies are considered as potential alternatives to estimate the voltage dip at the surrounding grid, which is the primary concern for E.ON. For the grid analysis part, PSS/E Xplorer 35.3 (which is a free limited version) is utilized because PSS/E is the preferred tool at E.ON for steady-state and short-circuit calculations. All the strategies are compared and evaluated for a hypothetical energization of a distribution transformer in a reduced network correspondent to the Öland island. Some results coincide with historical data from a similar distribution network, but on-site measurements or dynamic grid studies must validate the results. The in-built Python API[1] of PSS/E allows automating the process and incorporating it with the rest of the program.

As a result of this MSc Thesis, E.ON engineers will be able to use a friendly interactive tool that simulates with high accuracy the energization of a simplified three-phase transformer model and estimates the possible effect on the surrounding grid. However, they must be aware of the limitations and assumptions to make suitable sizing decisions.

[1] Application Programming Interface

This page is intentionally left blank

Contents

List of Tables

List of Figures

This page is intentionally left blank

1 Introduction

This first chapter aims to give a general understanding of the motivation for this MSc Thesis and the goals achieved. It presents the coming chapters and their contents, methodology, and insight into previous research.

1.1 Problem Definition

Increased demand for connection of renewable energy to the grid require innovative solutions from grid operators. When performing a grid connection study, several parameters are evaluated, amongst which is power quality. One of the main factors in determining power quality is voltage variations. When a transformer is energized, a current inrush is drawn from the grid to establish the magnetic field in the transformer. The magnitude and duration of the inrush current depend on several factors such as the size of the transformer and the strength of the network to which the transformer is being connected. To limit the disturbances that the energization of transformers may cause, their size is often constrained to a certain ratio of available short-circuit capacity[2]. This restriction comes from the fact that the larger the transformer is, the greater the inrush current and the deeper the voltage in the surrounding grid goes. Consequently, the decision to use multiple transformers instead of a large one to fit a new plant capacity impacts the project's budget and may determine its success.

As E.ON has a general guideline on transformer sizing that indicates that the maximum rated power of the transformer has to be less than **one tenth** of the short-circuit capacity of the bus at which the substation connects, which is often limited at the remote locations where new generation is installed, there is an appeal for the optimization of transformer sizing to each distinct situation by precisely simulating the voltage dip produced at the energizing bus and surrounding grid, and comparing it with present grid standards.

1.2 Goals

1. **Analyse the factors that determine the magnitude and duration of the transformer inrush.** This task involves modelling the dynamic equations that govern the transformer electrical properties during energization.
2. **Determine the impact of transformer inrush in the network considering power supply quality standards.** This task aims to determine how much it is possible to increase the transformer size of a transformer without compromising energy quality at a the surrounding grid.

[2]It is a parameter that measures how resilient the grid is under disturbances at a specific bus, expressed by the amount of current that flows on the system during a fault. Usually indicated in MVA, kVA or kA.

3. **Develop a tool for transformer connection studies.** It must be designed a Python-based user-friendly GUI[3] that uses some user input parameters regarding the transformer properties and connection and returns the necessary information to make a proper sizing decision.

1.3 Methodology

Inrush currents during transformer energization are a well-known issue extensively described in literature. Hence, modelling the equations that define its dynamics is a matter of understanding the different phenomena involved and making suitable assumptions. The next step is to find out the effect on the connected network, which relies on the PSS/E software because it is the main tool utilized at E.ON. The fact that is going to be used a phasor program to estimate a transient effect is one of the challenges of this MSc Thesis and a limitation imposed by E.ON as they do not provide other software licenses.

Other tools with superior transient analysis simulation such as Matlab Simscape or PSCAD are used for the validation of the transformer model designed in a Python (version 3.9) environment.

1.4 Knowledge Base

As mentioned before, transformer magnetizing inrush is a well-known physical phenomenon. There has been much research on this topic to avoid and mitigate adverse transient effects, such as voltage dips, malfunction of protection relays, considerable stresses over transformer, or interference in the operating condition of nearby electrical instruments [1, 2]. The assessment of this and similar problems over the years provides a good starting point to understand the transformer inrush dynamics with reasonable accuracy [3, 4, 5]. Concerning the simulation of inrush effects in the electric network, some found publications experiment with Matlab [6, 7, 3] and EMTP[4]-like programs such as PSCAD [8, 9], but there is no obvious reliable evidence of previous simulations of this kind using PSS/E.

1.5 Outline of the Thesis

The thesis problem can be divided in two main parts. The first one (Chapters 3.3 to 6) corresponds to the core of the report and is focused on the modelling of the transformer energization phenomenon. The second part (Chapter 7) is meant to analyze the impact of transformer energization in the grid using PSS/E and the results from the Python simulation. Finally, the transient and steady-state parts need to be coordinated by a programmed interface for E.ON use in grid connection studies (Chapter 8). Additionally, an introductory theory chapter is included in Chapter 2.1, as well as a brief overview of the problem in Chapter 3.2.

[3] Graphical User Interface
[4] Electromagnetic Transients Program

2 Transformer Energization

The transformer is a crucial aspect in the development of electric energy that require analyzing electric and magnetic circuits to comprehend its working principle. In general, magnetic variables such as magnetic field and flux density are functions of space and time determined by the geometry of the conductors and the magnetic structure, by the properties and history of the magnetic material, and by the values and derivatives or frequencies of the currents. Therefore, a problem involving non-linear behaviours is encountered [10].

One source of poor power quality is the disturbances caused by transformer energization, which can result in large amounts of currents absorbed by the transformer due to the non-linearity of the magnetic material in its core. This effect causes damage not only to the transformer itself but also to the rest of the system [11]. Chapter 2.1 explains how this phenomenon is produced.

The simulation of electromagnetic transients in power systems is essential for the adequate design of equipment and its protection. Therefore, transformer models are required for studying inrush currents where iron core nonlinearities play a vital role [12]. The main challenge is to develop a mathematical model with limited available data for this kind of study and defining the parameters of non-linear behaviours that are difficult to generalize and estimate.

2.1 Theoretical Basis

The transformer is an element with the ability to adapt voltage to the individual requirements of the different parts of the system. This faculty is derived from the fact that it is possible to magnetically couple the windings of the transformer in such a way that the turn ratio between them determines their voltage and inverse current ratio, resulting in the input and output energy being almost identical [13]. In Figure 1, the magnetic coupling concept is shown for two typical transformers.

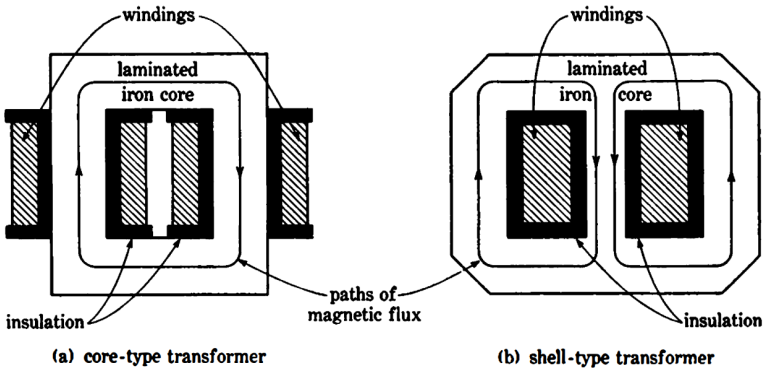

Figure 1: Magnetic structures of typical transformer [10]

The voltage conversion of transformers is accomplished at the expense of an exciting or magnetizing current that represents the energy loss required for the transformation. This is said to be exclusively dependent on the core design and material, which means that the excitation characteristics of a

transformer can be calculated without reference to the windings [13]. Power system engineers usually recognize exciting currents in the form of curves that relate them to the magnetic flux in the core. These curves are known as saturation curves, just like the one in the upper right corner of Figure 4.

The energization of a transformer (Figure 2) is simply a switch-in procedure usually performed with the secondary winding unloaded.

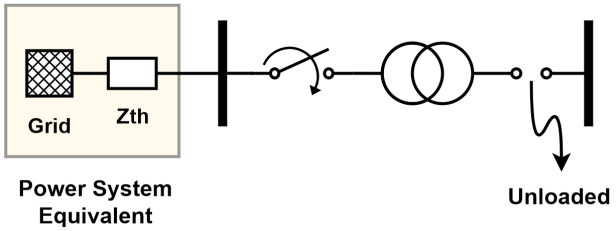

Figure 2: Energization of unloaded transformer (single-phase or three-phase)

In a power-system transformer with no load, the voltage drop v at the primary winding terminals is mainly defined by the counter electromotive force e induced by the changing flux φ:

$$v = e = N_1 \cdot \frac{d\varphi}{dt} = \frac{d\lambda}{dt} \tag{1}$$

Where,
N_1 is the number of turns of the primary winding
λ is defined as the flux-linkage

If the waveform of the applied voltage v is sinusoidal, the waveform of the flux must also be:

$$\lambda = N_1 \cdot \varphi_{max} \cdot sin(\omega t) = \lambda_{max} \cdot sin(\omega t) \tag{2}$$

by differentiation:

$$e = \omega \lambda_{max} \cdot cos(\omega t) \tag{3}$$

This means that, in steady-state operation, the induced voltage leads the flux by 90 degrees, as depicted in Figure 3.

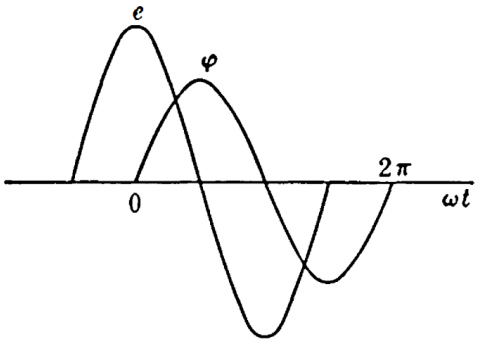

Figure 3: Phase relations of flux and induced voltage [14]

If a transformer could be switched in at the instant of the voltage wave, which normally corresponds to the residual magnetic flux in the core, switching in would be a smooth continuation of a previous operation without giving rise to a magnetic transient. But, in practice, the instant of switching in is not under control. Therefore, a magnetic transient is practically unavoidable since the magnetic flux cannot be instantly created or destroyed [13]. This transient phenomenon occasionally causes high inrush currents characterized by asymmetrical waveforms that are damped in some tens of cycles primarily by the series resistances of the systems.

To properly understand the formation of inrush currents, let's suppose that the transformer is energized when the voltage wave crosses zero as it rises and that the residual flux in the core is λ_0. Then, flipping Equation 1 we have that:

$$\lambda = \int v dt + \lambda_0 \tag{4}$$

In consequence, the flux-linkage will reach a maximum theoretical value of $2\lambda_{max} + \lambda_0$. Notice that, if λ_0 is equal to $-\lambda_{max}$, as it would have been in steady state (see Figure 3), the maximum value would be $2\lambda_{max} - \lambda_{max} = \lambda_{max}$, which is consistent.

The problem with reaching higher flux-linkage values than in normal operation is that the ferromagnetic material of the core may become saturated, reaching a point in the saturation curve where the magnetizing current can reach several times the nominal current of the transformer. A qualitative and simplified representation of the inrush current phenomenon is illustrated in Figure 4 for energization at voltage zero crossing.

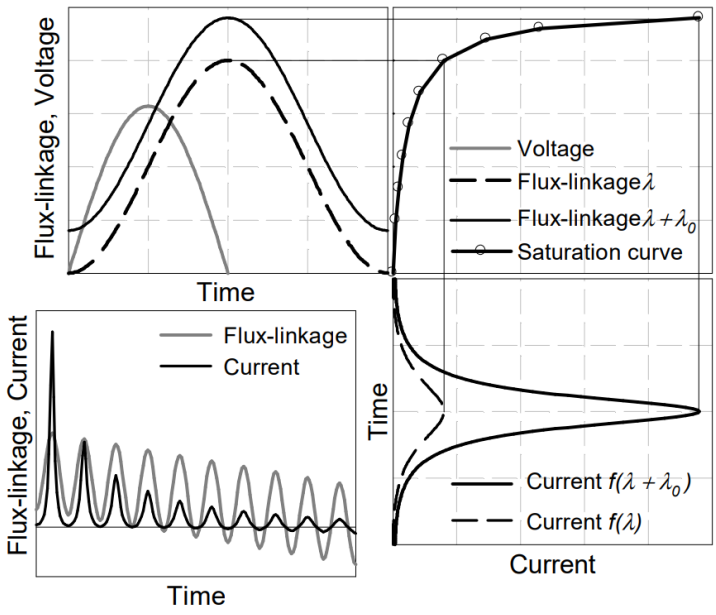

Figure 4: Qualitative representation of the inrush current phenomenon [5]

Inrush currents can also be produced in other circumstances, such as sympathetic interaction with nearby transformers, out-of-phase generator synchronisation, external faults and fault clearance.

However, the energization of a transformer typically yields the most severe case of inrush current. [5].

Potential problems related to the reduction of power quality due to transformer energization include voltage dips, temporary overvoltages and misoperation of protection relays, which are discussed in detail in Chapter 7.

As it has been explained, the magnitude of inrush currents are highly subjected to the voltage point at the energization time and residual flux of the transformer. Therefore, different scenarios are compared in the Appendix A for a better understanding of the phenomenon.

3 Modelling and Simulation Approach

This chapter intends to give some perspective to the problem addressed in this MSc Thesis and introduce the fundamentals for transformer modelling.

3.1 Modelling and Simulation Tools

The project's core relies on Python, a friendly and easy-to-use open-source programming language. The GUI, transformer model and energization simulation are all programmed in Python, and Matlab and PSCAD are only used during the design process to verify that the simulations and models are correct. PSS/E Xplore 35.3 (a free limited version) is utilized to estimate the voltage dip at nearby buses and is controlled automatically by commands written in Python. Additionally, to generate the transformer model, Python collects data from a PSS/E *.sav* file according to the user's instructions.

3.2 Problem Overview

How to satisfy the three goals explained in Chapter 1.2 is not a trivial answer, and understanding the procedure properly is useful to appreciate some important decisions later on.

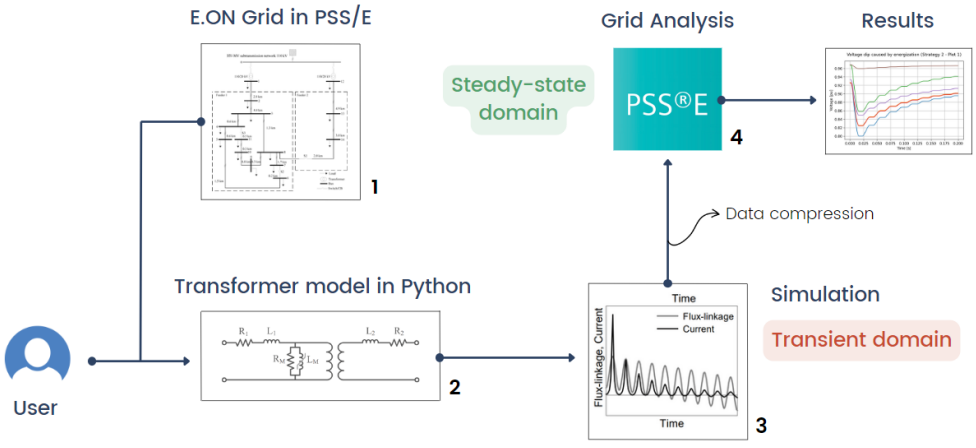

Figure 5: Overview of the problem

The required steps in order to achieve all the objectives are schematically presented in Figure 5:

1. The user provides enough information regarding the location of the transformer in the grid and its properties.
2. With the information from the user, the transformer model is built in a Python environment.
3. The energization phenomenon is simulated and time data is stored for later processing.

4. Finally, using the compressed data from the simulation and PSS/E software, the impact in the grid is analysed.

All four steps are embedded in a Python program coordinating all required processes and visuals. The user interface will ask for information at the start, and results will be shown when all steps are finalised. One important characteristic is the independence of each step: every stage begins when the preceding one ends (two steps are never run in parallel). Since Matlab and PSCAD are used for verification during the model design, they do not play any role after the program is finished, and hence they do not appear in Figure 5.

3.3 Transformer Modelling Fundamentals and Scope

The first step in the modelling process is to learn what are the different options that have been used in previous investigations and categorize their advantages and disadvantages. Because energizing a transformer is a transient phenomenon, Table 1 summarizes the different types of transients:

Transient type	Temporary	Slow Front	Fast Front	Very Fast Front
Frequency range	0.1 Hz to 1 kHz	50 Hz to 10 kHz	10 kHz to 1 MHz	100 kHz to 50 MHz
Example	Ferroresonance	Switching events	Lightning	Disconnector switching in GIS

Table 1: Classification of frequency ranges for the simulation of power system overvoltages [15]

According to [5], the frequency of interest for transformer energization studies ranges from DC[5] up to 1-3kHz, meaning that the guidelines for its model are those recommended for analysis of temporary or slow front transients. However, a unified and generally accepted model for transformers capable of reproducing their behaviour under all low-frequency operating conditions does not exist. The most typical models are now commented:

- **Saturable Transformer Component (STC Model):** this model, represented in Figure 6a, is the most manageable and elementary of all the presented alternatives. There is also a three winding version of this model, but it can be numerically unstable in some occasions. The most significant limitation when used to model three-phase transformers is that the inter-phase magnetic coupling is not represented, which is important for studying unbalanced operation.

- **Pi-equivalent or matrix representation (BCTRAN Model):** this type is somewhere in between the classic STC model and the more advanced models. It has the advantage of being stable for three winding transformers, include inter-winding coupling, and consider simplified inter-phase coupling; but because it is a linear model there are some difficulties in representing saturation and hysteresis effects, meaning that they have to be usually attached externally to the terminals. All core designs have the same mathematical treatment.

- **Topological models (UMEC/Hybrid Transformer Model):** there are different options of this type that have tried to address the problems of simpler models. They are commonly used when there is a special need for accuracy, and they can take into account the core construction topology. They are designed considering the duality between the electric and

[5]Direct Current (0 Hz)

magnetic circuit, and they are very precise when simulating highly nonlinear and unbalanced electromagnetic transients. The main drawback is the amount of input information required to build the model, usually not known by the power system engineer. Therefore, due to the the limited information that engineers at E.ON will have available and to reduce the complexity, topological models are immediately rejected. An example of the Hybrid Transformer Model is shown in Figure 6b.

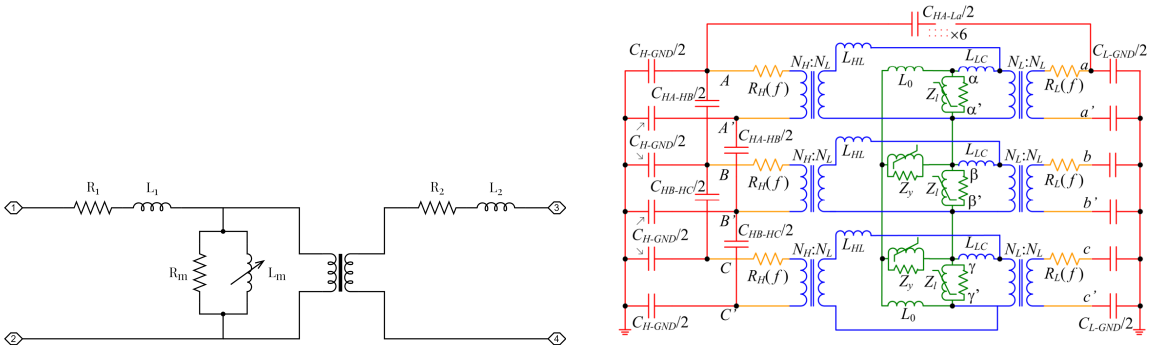

(a) STC model **(b)** Hybrid transformer model [16]

Figure 6: Two types of transformer models

To model the transformer energization in detail, the following aspects need to be represented (in order of importance) [5]:

1. Leakage impedance and winding resistance
2. Nonlinear saturation
3. Air-core inductance
4. Magnetic phase coupling
5. Residual flux
6. Frequency dependent winding losses
7. Zero sequence impedance
8. Hysteresis and frequency dependent iron losses
9. Capacitances

In general, to model the **capacitances (9)**, the **magnetic phase coupling (4)**, and the **zero sequence impedance (7)**, topological models are required. This means that, unfortunately, these aspects will not be represented in the model.

With respect to **frequency dependent winding losses (6)**, a Foster equivalent circuit can be used for an accurate representation of the winding resistance and the leakage inductance in low-frequency and switching transients. To obtain parameters of such circuit, a frequency response test

must be performed and a fitting procedure applied, or use approximations from reliable literature [15]. As the designed tool should be as general as possible, and this type of information will not be available for the users, it has been decided to neglect the frequency dependency of the winding losses.

When the flux in the iron core is reversed, the operating point in the saturation curve does not follow the same trajectory as when it was building up. This phenomenon is known as the **hysteresis (8)** effect and it depends on the immediate past history of the flux variation. As a result of hysteresis, the plot of flux versus current is no longer a single curve. In steady-state operation, the plot is almost a symmetric loop (Figure 7), whereas in transient state it can have much more complicated shapes. Advance models to represent this nonlinear, history and frequency dependent phenomenon are complex (but accurate) and their parameters are hard to obtain. Although there are easy methods to determine simplified hysteresis curves, its effect is negligible and it will be only useful for estimating residual flux values, which can also be done with literature.

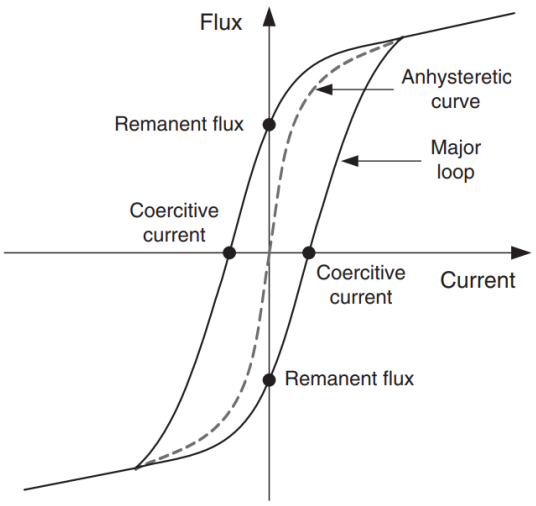

Figure 7: Hysteresis curve [15]

Frequency dependent iron losses (8) include hysteresis losses and eddy current losses, and can be represented by a constant resistor in parallel with the magnetizing inductance branch. This is reported to be accurate within 5% up to about 3 kHz [17]. When a transformer is subjected to a transient, the induced eddy currents are beneficial because they add damping. For practical purposes, when frequency dependency is neglected it is safe to say that the duration if not the amplitude of the resulting current is overestimated [5].

In summary, due to modelling limitations and simplifications, from the initial list only these are taken into account in the following chapters:

- Leakage impedance and winding resistance
- Nonlinear saturation
- Air-core inductance
- Residual flux

4 Modelling of Single Phase Transformers

Before describing the model in detail, it is a friendly beginning to show an initial perspective by reducing the problem to its simplest form, which can be very useful to extract some basic conclusions and intuition.

Using the STC model in Figure 6a and considering that no current is flowing through the secondary winding, plus the magnetizing inductance is assumed invariant, it is possible to use an equivalent RL circuit to represent the transformer.

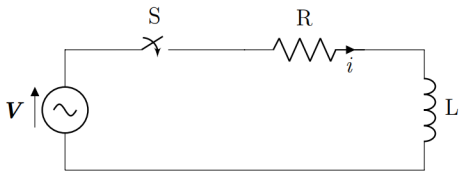

Figure 8: RL circuit [18]

Notice how the parallel magnetizing branch in winding one is transformed into an equivalent series resistance and inductance, and that they are later merged with the winding resistance and inductance. Afterwards, an ideal voltage source is added to the terminals. The dynamics of an RL circuit are based on the following differential equation:

$$V = V_m \cdot sin(wt + \theta) = Ri + L\frac{di}{dt} \tag{5}$$

Equation 5 is a first order ordinary linear differential equation that can be solved analytically using different mathematical methods. Without digging in detail on how this is done, it is relevant to say that any equation of this type has a steady-state and transient term solution. The second decays to zero with time, meaning that eventually only the steady-state term will remain.

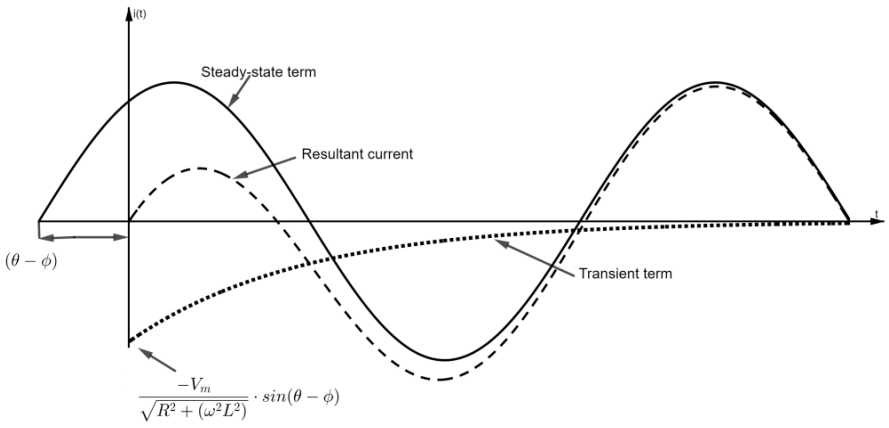

Figure 9: Transient response of an RL circuit [18]

The solution to Equation 5 is:

$$i(t) = \frac{V_m}{\sqrt{R^2 + (w^2 L^2)}} \cdot \left[sin(wt + \theta - \phi) - e^{-\alpha t} \cdot sin(\theta - \phi) \right] \tag{6}$$

Where,
V_m is the amplitude of the voltage source
α is the time constant given by the relationship R/L
θ is the initial angle of the voltage

Even if this methodology does not represent the actual scenario, it is interesting to mention that previous researchers have proposed similar equations with empirical coefficients that seek to find the inrush current peaks [5]. Some of this equations are compared in Figure 10.

A relatively simple equation given by Bertagnolli with very visible resemblance is:

$$i_n = \frac{V_m}{\sqrt{R^2_{winding} + (w^2 L^2_{air-core})}} \cdot \left(\frac{2B_N + B_R - B_S}{B_N} \right) \cdot e^{-\alpha t_n} \tag{7}$$

Where,
B_N is the rated flux density in the core (peak value)
B_R is the residual flux density in the core
B_S is the saturation flux density

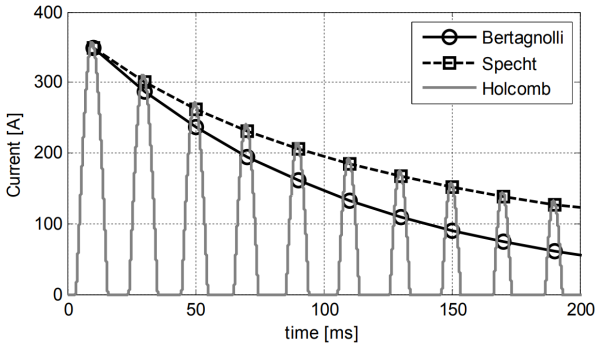

Figure 10: Comparison of equations for analytical estimation of inrush current [5]

4.1 Equivalent Electric Circuit

Directly from the STC model (see Figure 6a), and moving the elements in the secondary winding to the primary side, is obtained the equivalent single-phase circuit, depicted in Figure 11, commonly known as the traditional (Steinmetz) T-equivalent model, which has been generally accepted for longer than a century.

This representation requires certain assumptions that are not entirely correct. For instance, the leakage reactance is partially divided by the first and secondary winding, but it is only possible

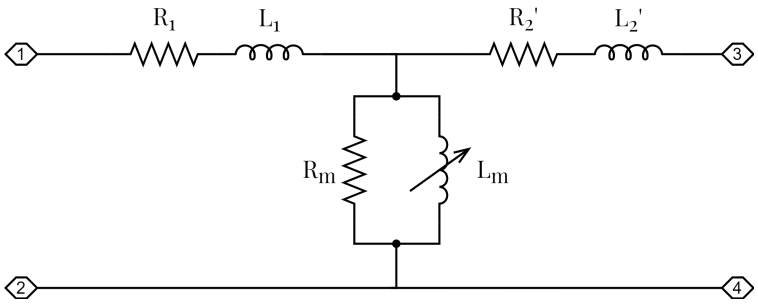

Figure 11: Equivalent T circuit

to measure it as a whole (for a pair of inductors), which brings uncertainty on how the division should be carried out. Also, reasonable errors in the T-equivalent model have been identified while simulating heavy saturation conditions, which can be a limiting condition for such type of studies. A similar model that better represents the physical meaning of the transformer elements is the Π-equivalent circuit in Figure 12, obtained from the principle of duality between magnetic and electric circuits. When duality is applied to a single-phase transformer, the resultant model has only one leakage inductance branch in series and two shunt magnetizing branches. It is interesting to mention that both models are absolutely the same when the magnetizing branch is neglected, very common in steady state and short-circuit calculations [19].

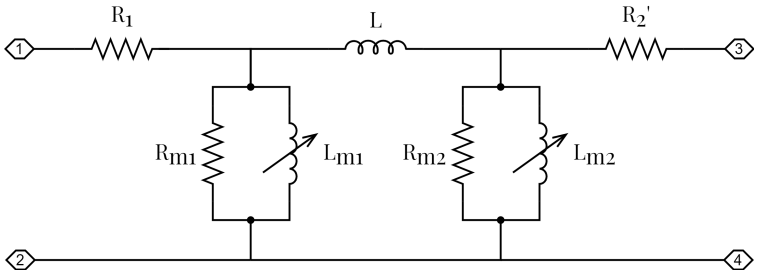

Figure 12: Equivalent Π circuit

Despite the possible advantages of using the Π model, it clearly adds an extra difficulty. In the first place because the mathematical differential equations are of a higher order, the different branches make the algebraic expressions more complex, and modelling saturation is less obvious as there are two independent magnetizing inductances; and secondly because the verification tools at hand only have available the classic Steinmetz model and other specific topological models. These are the main reasons why it has been decided to use the common T-equivalent model.

Regarding the splitting of the winding resistance and leakage reactance, in [5] is mentioned the following: "A 50% splitting factor is often used. However, it should be more accurate to put 75% – 90% of the leakage inductance on the HV[6] side and the rest on the LV[7] side, as the leakage inductance between the HV winding and the core is normally larger than the one between the LV winding and the core. In energization studies this results in a larger inrush current in p.u. on the LV side than on the HV side as observed in practice". However, because PSCAD also recommends using a 50% division, it has been decided to do so. This is not a serious simplification because

[6]High Voltage
[7]Low Voltage

using a smaller inductance will, at any case, produce a larger inrush current; meaning that the most extreme case is analysed.

4.2 Iron Core Nonlinearities and Residual Flux

The major iron core nonlinear effects are saturation, hysteresis, and eddy currents. From all, saturation is the predominant one, and because of the reasons exposed in Chapter 3.3, it is the only nonlinearity contemplated.

In most common studies, saturation non linearities are not considered because the transformer never reaches the saturated region, implying that the flux linkage and current have a linear relationship. However, during energization the transformer may become saturated due to a sudden change in the voltage applied to it; meaning that the saturation curve, which defines the instantaneous flux linkage λ as a function of current i, becomes an essential part for modelling the iron core nonlinearities.

There are different ways to include saturation in the model. The most common technique is to consider a constant magnetizing inductance correspondent to the unsaturated region L_M and a parallel current source i_s to account for the extra current absorbed in the core when saturated (Figure 13a). Then the saturation curve (Figure 13c) is used to estimate the current i_s for a previously calculated flux linkage λ_m as:

$$i_s(\lambda_m) = i_m(\lambda_m) - \frac{\lambda_m}{L_M} \tag{8}$$

The algorithm used in PSCAD is shown schematically in Figure 13b.

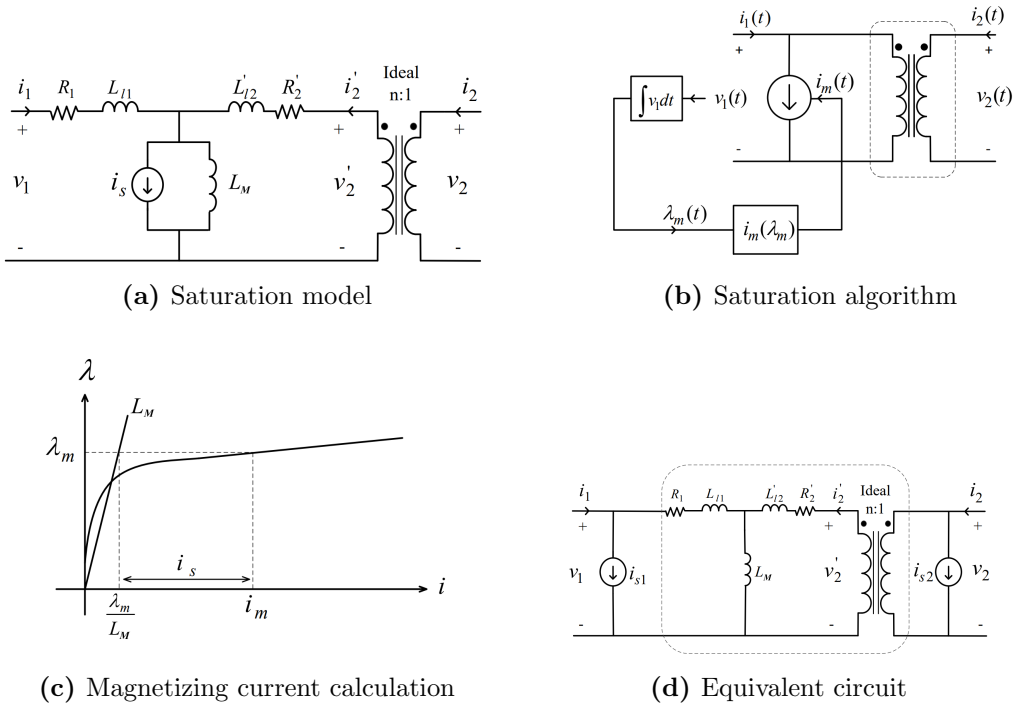

(a) Saturation model

(b) Saturation algorithm

(c) Magnetizing current calculation

(d) Equivalent circuit

Figure 13: PSCAD saturation approach [20]

Usually, when saturation is modelled using a current source, this is placed as an external element connected to one of the terminals. The benefit of this method is that internal nodes of the transformer are not added to the total number of nodes in the system. On the other hand, the position is shifted from the true location and it will cause inaccuracies. For this reason, an advanced equivalent model is commonly used, where a second current source inserted at the opposite terminal compensates the error (Figure 13d). The current source representation makes the model computationally efficient comparing to modeling with a nonlinear inductance, especially because the calculation of inverse matrices, typical in EMTP programs, would be otherwise required at every time step [20].

As efficiency is important but simplicity is preferred, a different and simpler method for modelling saturation is now presented.

The saturation curve (Figure 14) is built following the PSCAD method:

$$i_m = \frac{\sqrt{(\lambda_m - \lambda_K)^2 + 4DL_{air-core}} + \lambda_m - \lambda_K}{2L_{air-core}} - \frac{D}{\lambda_K} \tag{9}$$

Where,

$$D = \frac{-B - \sqrt{B^2 - 4AC}}{2A}$$

$$A = \frac{L_{air-core}}{\lambda_K^2}$$

$$B = \frac{L_{air-core} \cdot L_M - \lambda_M}{\lambda_K}$$

$$C = I_M \cdot (L_{air-core} \cdot I_M - \lambda_M + \lambda_K)$$

$\lambda_M = \frac{V_M}{2\pi f}$, being V_M the RMS rated voltage of the winding

$\lambda_K = K \cdot \lambda_M$, being K the knee point in p.u.

$L_M = \frac{\lambda_M}{I_M}$, being λ_M and I_M the peak magnetizing flux and current at rated voltage

*Note on **knee voltage**: the knee point of the saturation curve is sometimes available and is usually expressed in percent or per-unit of the operating point, defined by rated voltage. Typical ranges in per-unit are 1.15 to 1.25 [21]. The knee voltage is defined as the voltage at which a 10% increase in applied voltage increases the magnetizing current by 50%. If no information is known, the most severe case is chosen, which happens to be a knee voltage of 1.15 p.u.*

*Note on **air core inductance**: the air core inductance is represented by the straight-line characteristic, which bisects the flux axis at λ_K. The air core inductance may not be known. One rule of thumb is that air core reactance is approximately twice the leakage reactance in p.u. [21].*

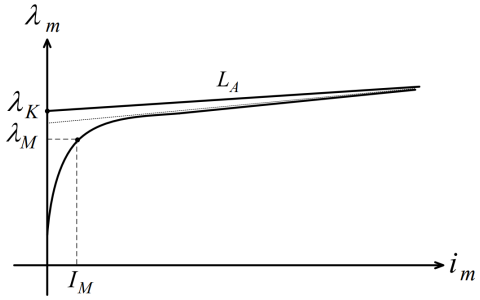

Figure 14: Core saturation characteristic of the classical transformer [20]. L_A refers to the air-core inductance and λ_K to the knee point. The curve is assumed to be odd symmetrical.

Then, the continuous saturation curve is converted to piecewise linear by selecting ten equidistant points between λ_M and $\lambda_K \cdot 1.05$. This transformation is shown in Figure 15. In most cases, only two sections are enough, but using more is justified because it provides smoother results and high accuracy.

The slope of the straight line between two consecutive points in the piece-wise linear curve is the magnetizing inductance of that region. Therefore, saturation is going to be modelled using a time-varying inductance that depends on the calculated flux-linkage across the winding at a specific time. This algorithm is shown schematically in Figure 16.

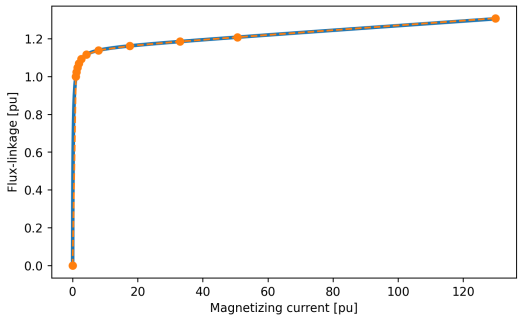

Figure 15: Piecewise linear saturation curve. Assumed to be odd symmetrical.

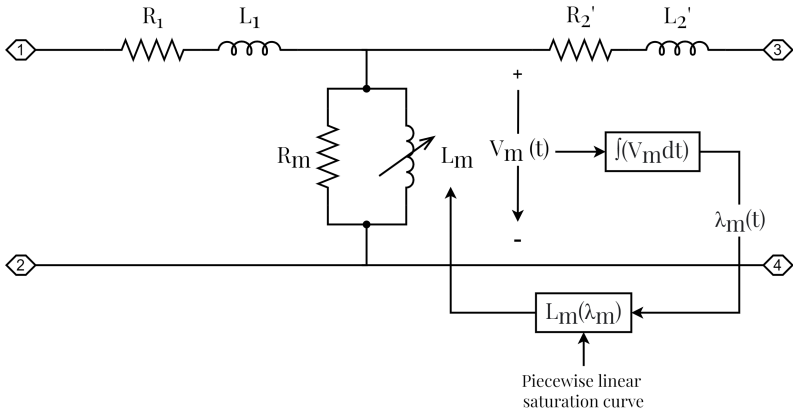

Figure 16: Proposed algorithm to model saturation

Finally, the residual flux λ_0 is modelled using an initial flux-linkage. Due to the ringdown transient, the residual flux is always somewhat lower than the theoretical maximum. According to [5], the residual flux can take any value between 0 and 0.8 times the rated value λ_M. Then, considering that the closing switch to energize the transformer is triggered when the voltage crosses zero, the initial flux that produces the most severe inrush current is 0.8 p.u. The residual flux is handled in more detail in Chapter 5.2.

4.3 Analysis of the Equivalent Electric Circuit and Computer Implementation

The equivalent circuit in its terminal form (Figure 11) must be completed with external elements representative of the energizing scenario:

- A network equivalent is added between the terminals 1 and 2 (HV winding). For that, is used an ideal voltage source in series with the positive thevenin impedance of the node at which the HV winding of the transformer is connected.
- Because the secondary winding is an open circuit when no load is connected, all of their elements are not participating in the phenomenon.

These boundary conditions are represented in Figure 17.

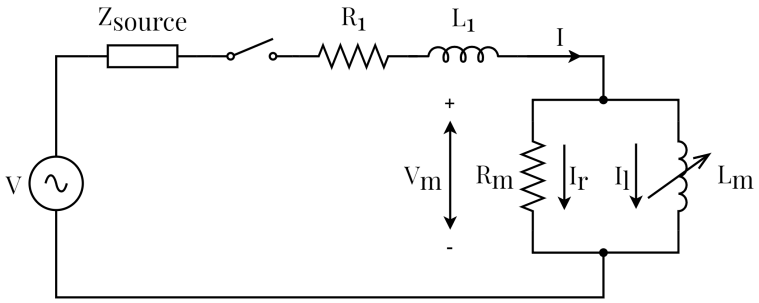

Figure 17: Single phase complete equivalent circuit

From now on, the source impedance Z_{source}, HV winding resistance R_1, and HV leakage reactance L_1 are merged into R and L for an easier mathematical formulation.

The objective is to find an expression similar to Equation 5 manipulating the relationship between variables. The physical equations are:

$$V = R \cdot I + L \cdot \frac{dI}{dt} + V_m \tag{10}$$

$$V_m = \frac{d\lambda}{dt} = L_m \cdot \frac{dI_l}{dt} = R_m \cdot I_r \tag{11}$$

$$I = I_l + I_r \tag{12}$$

Using Equations 10 and 11:

$$V = R \cdot I + L \cdot \frac{dI}{dt} + L_m \cdot \frac{dI_l}{dt} \tag{13}$$

From Equations 11 and 12:

$$I = I_l + \frac{L_m}{R_m} \cdot \frac{dI_l}{dt} \tag{14}$$

Finally, combining Equations 13 and 14:

$$V = A \cdot \frac{d^2 I_l}{dt^2} + B \cdot \frac{dI_l}{dt} + C \cdot I_l \tag{15}$$

Where,

$$A = \frac{L \cdot L_m}{R_m} << 1$$
$$B = \left(\frac{L_m R}{R_m} + L + L_m \right)$$
$$C = R$$

The A coefficient can be considered negligible because the value of R_m is often very large [20], meaning that Equation 15 can be rewritten as:

$$V = B \cdot \frac{dI_l}{dt} + C \cdot I_l \tag{16}$$

Equation 16 has exactly the same structure as Equation 5. The difference is that, in this case, the coefficient B is non-linear because L_m varies during the time. This alteration is in principle unpredictable, and the only way to solve this equation is by resorting to numerical methods. The easiest numerical method is possibly the Euler method, but even if it is very easy to implement, its little efficiency requires very small time steps to reach reasonable preciseness. For this reason, higher order methods, such as the classical Runge-Kutta, are frequently used for accurate computations. For the specific case of electromagnetic transient programs, discretizing the differential equations using the Trapezoidal Rule of Integration is recommended in [20, 15, 22].

4.3.1 Trapezoidal Rule of Integration

The simple Trapezoidal Rule is based on approximating a function $f(x)$ by the straight line joining $(a, f(a))$ and $(b, f(b))$. By integrating the formula for this straight line, we obtain the approximation. It averages the Euler and backward Euler methods, advancing the approximate solution at each time step.

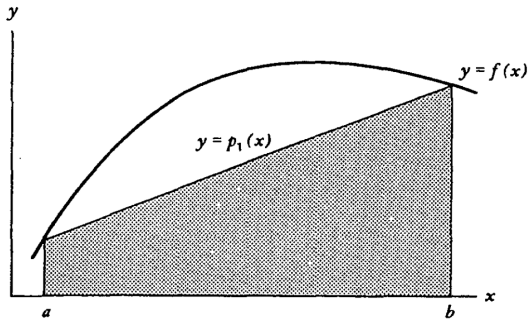

Figure 18: Illustration of the trapezoidal rule [23]

To solve an ODE of the shape $y' = f(t, y)$, the trapezoid method approximates the solution $y(t_{k+1})$ at time $t_{k+1} = t_k + \Delta t$ by solving the implicit equation [24]:

$$y_{k+1} = y_k + \frac{\Delta t}{2} \cdot [f(t_k, y_k) + f(t_{k+1}, y_{k+1})] \tag{17}$$

Applying this concept to Equation 16 and solving for $I_{l(k+1)}$ we have:

$$I_l' = f(t, I_l) = \frac{V}{B} - I_l \cdot \frac{C}{B} \tag{18}$$

$$I_{l(k+1)} = I_{l(k)} + \frac{\Delta t}{2} \cdot \left[\left(\frac{V_k}{B} - I_{l(k)} \cdot \frac{C}{B} \right) + \left(\frac{V_{k+1}}{B} - I_{l(k+1)} \cdot \frac{C}{B} \right) \right] \tag{19}$$

...

$$I_{l(k+1)} = \frac{1}{1 + \frac{\Delta t}{2}\frac{C}{B}} \left[I_{l(k)} + \frac{\Delta t}{2} \cdot \left(\frac{V_k}{B} - I_{l(k)} \cdot \frac{C}{B} + \frac{V_{k+1}}{B} \right) \right] \tag{20}$$

Notice that, even if B is considered a constant coefficient in the operations involving Equations 18 to 20, recall that it can change at any time depending on the operating point in the piecewise linear saturation curve (as it is a function of L_m). To know the instant value of B, we need to know first the flux-linkage. According to the proposed algorithm to model saturation, and using Equation 11, it is deduced that:

$$\lambda_m = \int V_m dt = \int \left(L_m \cdot \frac{dI_l}{dt} \cdot \right) dt = \int L_m dI_l \tag{21}$$

$$\lambda_{m(k+1)} = \lambda_{m(k)} + L_m \cdot \left(I_{l(k+1)} - I_{l(k)} \right) \tag{22}$$

The problem with Equation 22 is that it is a closed loop where we need an unknown variable to calculate another one. Actually, any chosen path leads to the same situation. To solve this issue, it is necessary to break the algebraic loop and designate one variable to be one time step behind the actual time. Taking advantage of the *error* committed for considering B (and hence L_m) constant in the derivation of Equations 18 to 20, L_m is declared as the outdated variable. The previous decisions are even more justified if it is realized that L_m only changes a limited number of times (as there is a fixed amount of possible values that can have according to the piecewise linear saturation curve), meaning that in some way, it is more constant than any other variable.

The variable of interest is the magnetizing current I, that can be immediately calculated using Equation 14:

$$I_{(k+1)} = I_{l(k+1)} + \frac{L_m}{R_m} \cdot \frac{\left(I_{l(k+1)} - I_{l(k)} \right)}{\Delta t} \tag{23}$$

4.3.2 Programming Flowchart

The programming process is summarized in Figure 19, where the simulation can be stopped at a specific time or after a certain number of iterations.

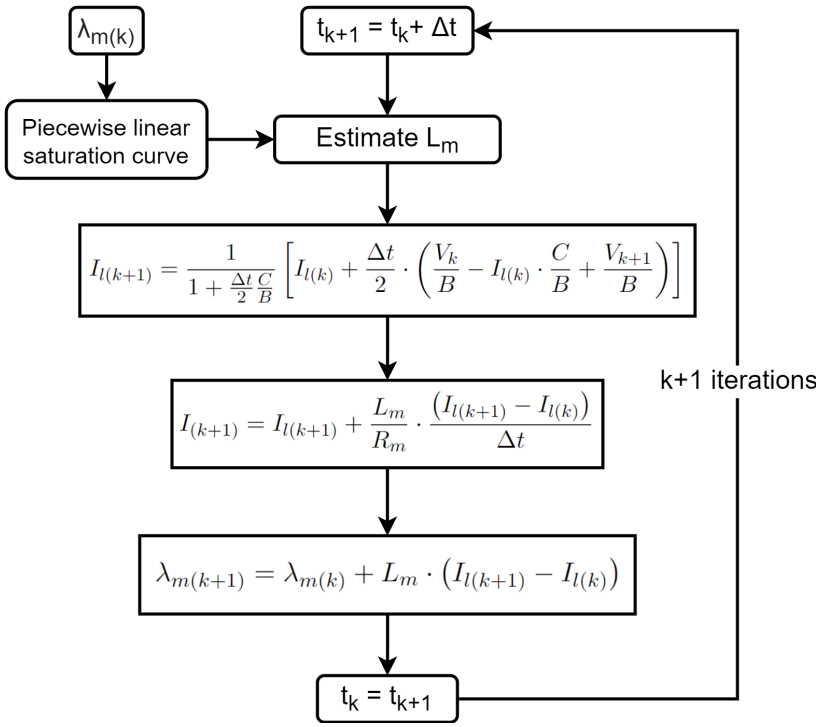

Figure 19: Flowchart of the designed computation technique

5 Modelling of Three Phase Transformers

In the previous chapter, it has been solved the mathematical problem of a single-phase transformer model when this is energized. To accomplish this task, the differential equations were discretized using the Trapezoidal Rule of Integration to obtain a step-by-step solution. In this new chapter, the approach for the single-phase problem is reutilized and expanded to the three-phase scenario.

Single-phase transformers are widely used in low voltage applications, but when it comes to the generation, transmission, distribution and industrial use of electrical power, three-phase transformers are dominant. When considering three-phase transformers, we have to deal with three alternating voltages and currents differing in phase-time by 120 degrees. Consequently, they add extra difficulty in solving the energization problem, especially when different phases influence each other.

5.1 Three Phase Transformer Overview

Treating three-phase transformers is much more complicated than the single-phase case. The different construction varieties make the interconnection between phases sophisticated and singular. Detailed models require geometrical details only available to manufacturers, and the idea is to simplify the problem by re-utilizing the single-phase model connecting three independent units in a *bank of three single-phase transformers*. In a transformer bank of single-phase units, the individual phases are not magnetically coupled, and their modelling is symmetrical where all three-phases have equal parameters.

The bank of three single-phase transformers can be connected in different ways, but the two most popular are Delta and Wye:

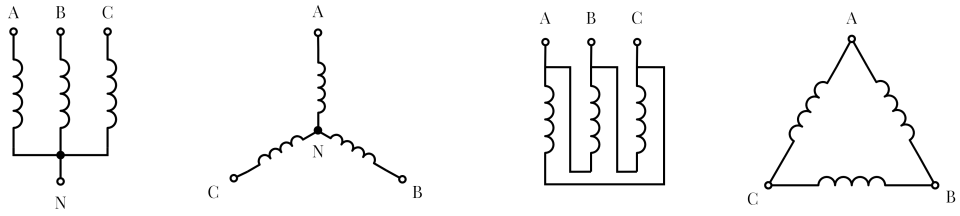

(a) Wye connection **(b)** Delta connection

Figure 20: Connection types diagrams

In Figure 20a, the grounding of the neutral point N affects the magnitude of the inrush current, and it is important to consider the different possibilities that E.ON may encounter in their grid. The most common combinations, considering connection type and grounding, are summarized in Table 2. Even if there are other possibilities, taking into account only those in which E.ON has special interest is a reasonable limit. The grounding in the secondary winding is not relevant in this case because the energization is performed at no load conditions.

HV side	LV side	Grounding (HV)
Wye	Wye	Directly grounded
Wye	Wye	Isolated
Wye	Delta	Directly grounded
Wye	Delta	Isolated

Table 2: Three phase transformer connection types considered and its grounding

For E.ON, when a transformer neutral is isolated, it means that there is a surge arrester connected between the neutral and ground to protect it from over-voltage transients. On the other hand, when a transformer neutral is directly grounded, it does not mean that there is no protection against over-voltage transients; instead, it is installed somewhere in the surrounding area.

5.2 Saturation and Residual Flux

In the single-phase model, the variable magnetizing inductance changes depending on the flux-linkage across it, just like it was said in Chapter 4.2. Now, each phase follows the same algorithm independently, meaning that one phase may become saturated while the others are not, leading to many different possible unsymmetrical scenarios. Because the bank of three single-phase transformers is modelled symmetrically, all phases share the same saturation curve.

The residual flux in each phase of the transformer core may depend on a number of factors, such as core type, neutral winding, circuit breaker, etc ... For simplicity, it is assumed that the transformer conditions prior to disconnection are no load at the secondary and steady-state operation. According to [5], "when the transformer is disconnected by the circuit breaker (which can occur at any time), the fluxes form a 120° phase-shifted balanced symmetrical set. Depending on the capacitances linking the transformer to the network and/or to the ground, these fluxes will decay and then stabilize at a certain value." This final value ranges between 0 and 80% of the rated flux. In statistical terms:

$$\lambda_0 = 0.8 \cdot \lambda_M \cdot U\,[0, 1] \tag{24}$$

$$\theta = U\,[0, 2\pi] \tag{25}$$

Where,

θ is the reference phase angle of the balanced symmetrical set of the residual fluxes
$U\,[a, b]$ represents a uniform distribution between a and b

Every phase has its own value for λ_0, and together with the reference angle θ, the residual flux of each phase is calculated as:

$$\lambda_h = \lambda_{0(h)} \cdot cos\left(\theta + (h-1) \cdot \frac{2}{3}\pi\right), h = 1, 2, 3 \tag{26}$$

By generating random samples of λ_0 and θ, one can obtain arbitrarily samples of three residual fluxes λ_h correspondent to phases A, B, and C. In [5], some potential flux values are directly given:

$$\{\lambda_A, \lambda_B, \lambda_C\} = \{0, 0, 0\} \tag{27}$$

with relative probability of 1/3

$$\{\lambda_A, \lambda_B, \lambda_C\} = \{1, -0.5, -0.5\} \cdot 0.8 \cdot \lambda_M \tag{28}$$

with relative probability of 1/9

$$\{\lambda_A, \lambda_B, \lambda_C\} = \{0.76, 0, -0.76\} \cdot 0.8 \cdot \lambda_M \tag{29}$$

with relative probability of 1/9.

The combination that causes the most severe inrush current is reflected in Equation 28. For this reason, it will be the default value used during the simulations providing that no other information is known.

5.3 Equivalent Electric Circuit

Assembling the equivalent electric circuit for a bank of three single-phase is straightforward. The one thing that requires special attention is to carefully connect the terminals of each independent single-phase model as in Figure 20 depending on the connection type. The grounding is not included in the equivalent circuit because it is defined externally at the terminal N of each model.

5.3.1 Wye/Wye connected transformer

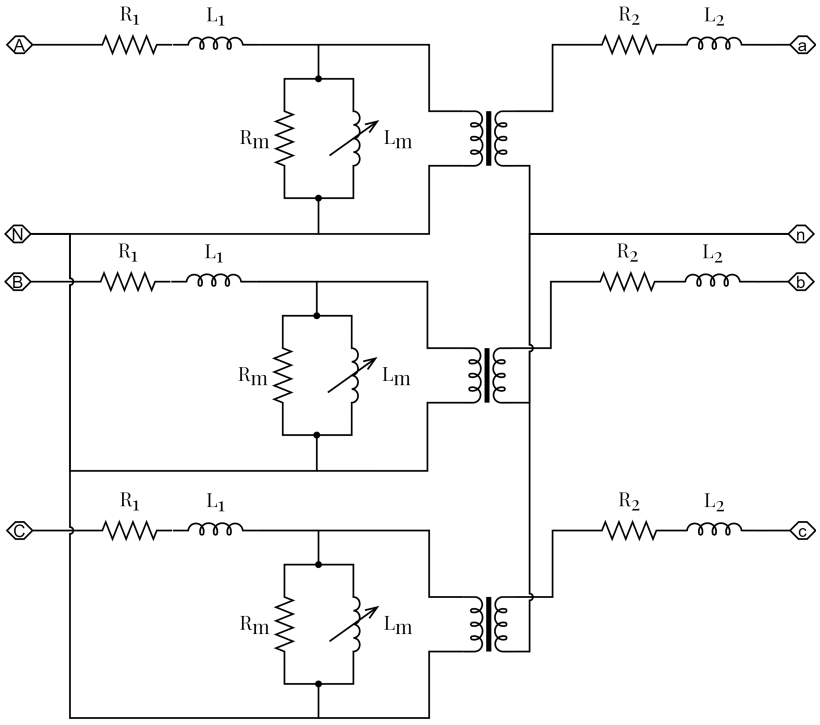

Figure 21: Bank of three single-phase transformers connected in Wye/Wye

Like in the single-phase case, when the secondary side is unloaded, its elements do not participate in the energization phenomenon because current cannot flow through them, as the LV terminals are disconnected from the system.

5.3.2 Wye/Delta connected transformer

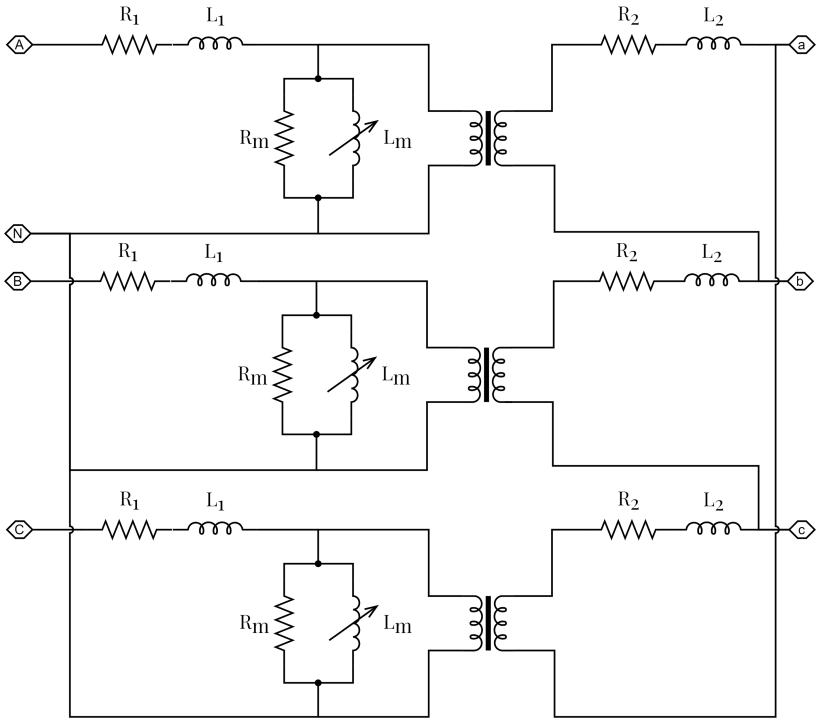

Figure 22: Three single-phase transformer bank connected in Wye/Delta

In contrast with the Wye/Wye connection, the secondary side has a Delta loop in which current can flow without escaping through the disconnected terminals a, b, or c. This implies that the elements R_2 and L_2 have an influence on the inrush current and should be taken into account in the analysis of the circuit.

5.4 Analysis of the Equivalent Electric Circuit and Computer Implementation

The mathematical formulation of the equivalent models is different depending on the connection and grounding type. Consequently, each combination in Table 2 has its own solution, although they have some things in common. In particular, the Trapezoidal Rule of Integration is utilized in all cases to discretize the differential equations. A new mathematical algorithm is also introduced as the characteristics of the mathematical equations demand it: The Newton Raphson Method. This algorithm, which allows the system of equations to converge, is explained in 5.4.2 because it is the first case where it is required, and other cases refer to the explanations in that section.

5.4.1 Wye/Wye connection with primary directly grounded

This is the easiest connection type to implement because, as the primary neutral is connected directly to ground, each phase can be interpreted as an independent circuit. This means that there is not interaction between phases in any way, allowing to use the same mathematical model as in Chapter 4.3. The only difference is that the voltage source should be properly defined for a symmetrical three-phase system, with each phase shifted 120 degrees with respect to the others.

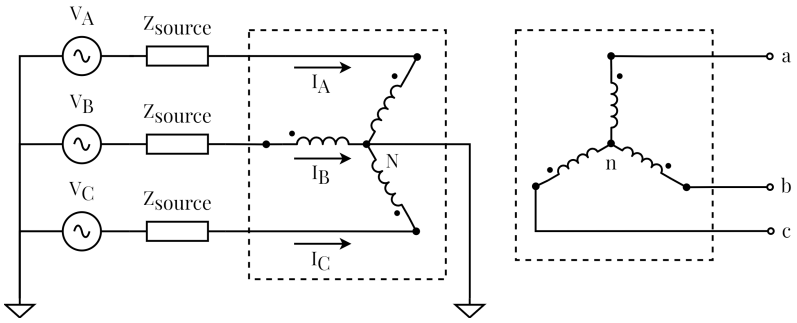

Figure 23: Three phase transformer in Wye/Wye connection with primary directly neutral grounded. The dashed squares mean that the three-phase transformer representation is simplified. The model is completed with Figure 21.

Because of the characteristics previously mentioned, three independent mathematical equations are enough to represent the model:

$$\begin{cases} V_A = R \cdot I_A + L \cdot \dfrac{dI_A}{dt} + \dfrac{d\lambda_A}{dt} \\ V_B = R \cdot I_B + L \cdot \dfrac{dI_B}{dt} + \dfrac{d\lambda_B}{dt} \\ V_C = R \cdot I_C + L \cdot \dfrac{dI_C}{dt} + \dfrac{d\lambda_C}{dt} \end{cases} \tag{30}$$

Where,

V_i refers to the phase voltage
$R = R_{source} + R_1$
$L = L_{source} + L_1$

The obvious relationship with the single-phase problem justifies no further explanations.

5.4.2 Wye/Wye connection with primary isolated (infinite ground resistance)

The main reason why there is an infinite resistance between the primary neutral and ground (Figure 24) is because it was numerically unstable to keep it isolated. In fact, the resistance to ground could not be greater than $1 \cdot 10^3\ \Omega$ in order to converge.

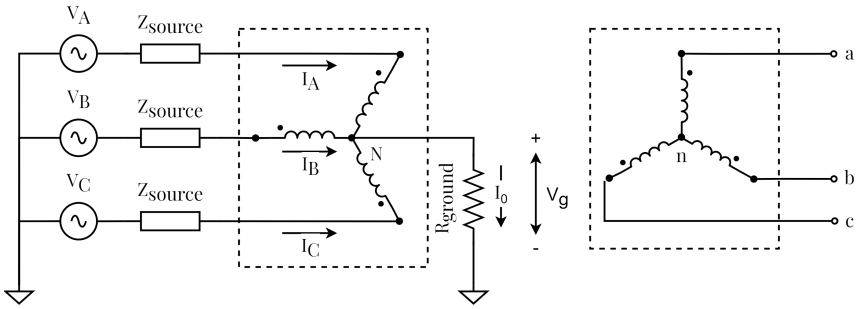

Figure 24: Three phase transformer in Wye/Wye connection with primary neutral isolated (infinite ground impedance). The dashed squares mean that the three-phase transformer representation is simplified. The model is completed with Figure 21.

The current I_0 that flows through the ground resistance R_{ground} is the sum of phase currents I_A, I_B, and I_C; and the voltage drop across it is V_g:

$$V_g = R_{ground} \cdot I_0 = R_{ground} \cdot (I_A + I_B + I_C) \tag{31}$$

In balanced operation, $I_A + I_B + I_C$ should be null, but the asymmetrical behavior typical of inrush currents can make the sum non-zero. If the neutral is fully isolated, the sum is forced to be zero as there is no path where the zero-sequence current could go. However, the necessity to place an impedance between neutral and ground opens that door. Still, because the resistance R_{ground} is of the order of a thousand, I_0 is expected to be very small.

Applying the Kirchhoff's Voltage Law (KVL) to the circuit in Figure 21 and rewriting it as in Equation 16:

$$\begin{cases} V_A - V_g = R \cdot I_A + L \cdot \dfrac{dI_A}{dt} + \dfrac{d\lambda_A}{dt} = B_A \cdot \dfrac{dI_{lA}}{dt} + C \cdot I_{lA} \\ V_B - V_g = R \cdot I_B + L \cdot \dfrac{dI_B}{dt} + \dfrac{d\lambda_B}{dt} = B_B \cdot \dfrac{dI_{lB}}{dt} + C \cdot I_{lB} \\ V_C - V_g = R \cdot I_C + L \cdot \dfrac{dI_C}{dt} + \dfrac{d\lambda_C}{dt} = B_C \cdot \dfrac{dI_{lC}}{dt} + C \cdot I_{lC} \end{cases} \tag{32}$$

Where,

V_J refers to the phase voltage with $J = A, B, C$

$R = R_{source} + R_1$

$L = L_{source} + L_1$

$B_J = \left(\dfrac{L_{mJ} R}{R_m} + L + L_{mJ} \right)$

$C = R$

The structure of Equation 32 is still very similar to the single-phase problem, but there is an important difference: the equations are not independent anymore because to define V_g, the solutions for I_A, I_B, and I_C are needed. This makes it a system of three dependent non-linear differential equations. Solving this mathematical problem requires an iterative solution method. From all

possible alternatives, the popular Newton-Raphson Algorithm is recommended in [22, 17], and will be implemented in this and following cases.

The solution of any equation $F(\mathbf{x}) = 0$ by the Newton method needs a good initial guess for satisfactory convergence (in each time step). In this case $F(\mathbf{x})$ is defined as:

$$F(\mathbf{x}) = \begin{cases} f_1(\mathbf{x}) = I_{lA(k+1)} - \dfrac{1}{1+\dfrac{\Delta t}{2}\dfrac{C}{B_A}}\left[I_{lA(k)} + \dfrac{\Delta t}{2}\cdot\left(\dfrac{V_{A(k)} - V_{g(k)}}{B_A} - I_{lA(k)}\cdot\dfrac{C}{B_A} + \dfrac{V_{A(k+1)} - V_{g(k+1)}}{B_A}\right)\right] \\ f_2(\mathbf{x}) = I_{lB(k+1)} - \dfrac{1}{1+\dfrac{\Delta t}{2}\dfrac{C}{B_B}}\left[I_{lB(k)} + \dfrac{\Delta t}{2}\cdot\left(\dfrac{V_{B(k)} - V_{g(k)}}{B_B} - I_{lB(k)}\cdot\dfrac{C}{B_B} + \dfrac{V_{B(k+1)} - V_{g(k+1)}}{B_B}\right)\right] \\ f_3(\mathbf{x}) = I_{lC(k+1)} - \dfrac{1}{1+\dfrac{\Delta t}{2}\dfrac{C}{B_C}}\left[I_{lC(k)} + \dfrac{\Delta t}{2}\cdot\left(\dfrac{V_{C(k)} - V_{g(k)}}{B_C} - I_{lC(k)}\cdot\dfrac{C}{B_C} + \dfrac{V_{C(k+1)} - V_{g(k+1)}}{B_C}\right)\right] \end{cases} \tag{33}$$

Where,

$\mathbf{x} = (x_1, x_2, x_3)$
$x_1 = I_{lA(k+1)}$
$x_2 = I_{lB(k+1)}$
$x_3 = I_{lC(k+1)}$

and f_1, f_2 and f_3 are obtained discretizing the expressions in Equation 32 using the Trapezoidal Rule of Integration.

The initial guess $\mathbf{x}^{(0)}$ can be estimated in a similar way as in Figure 19 and using outdated variables when necessary. Then, $\mathbf{x}^{(0)}$ is updated in an iterative way until it converges to a certain value $\mathbf{x}^{(n)}$ according to:

$$\mathbf{x}^{(i+1)} = \mathbf{x}^{(i)} - \left[Jac^{(i)}\right]^{-1} \cdot F\left(\mathbf{x}^{(i)}\right) \tag{34}$$

Where i is the iteration counter and Jac is the Jacobian matrix of $F(\mathbf{x})$:

$$Jac = \begin{bmatrix} \dfrac{df_1(\mathbf{x})}{dx_1} & \dfrac{df_1(\mathbf{x})}{dx_2} & \dfrac{df_1(\mathbf{x})}{dx_3} \\ \dfrac{df_2(\mathbf{x})}{dx_1} & \dfrac{df_2(\mathbf{x})}{dx_2} & \dfrac{df_2(\mathbf{x})}{dx_3} \\ \dfrac{df_3(\mathbf{x})}{dx_1} & \dfrac{df_3(\mathbf{x})}{dx_2} & \dfrac{df_3(\mathbf{x})}{dx_3} \end{bmatrix} \tag{35}$$

To derivate $F(\mathbf{x})$ with respect to x_j, it is necessary to write V_g in terms of I_{lA}, I_{lB}, and I_{lC} combining Equation 31 with Equation 14:

$$V_g = R_{ground} \cdot \left[\left(I_{lA} + \frac{L_{mA}}{R_m}\cdot\frac{dI_{lA}}{dt}\right) + \left(I_{lB} + \frac{L_{mB}}{R_m}\cdot\frac{dI_{lB}}{dt}\right) + \left(I_{lC} + \frac{L_{mC}}{R_m}\cdot\frac{dI_{lC}}{dt}\right)\right] \tag{36}$$

Going further into the details of the mathematical solution is not relevant to the reader. Instead, a explanatory flowchart in Figure 25 is presented to make clear all the required steps.

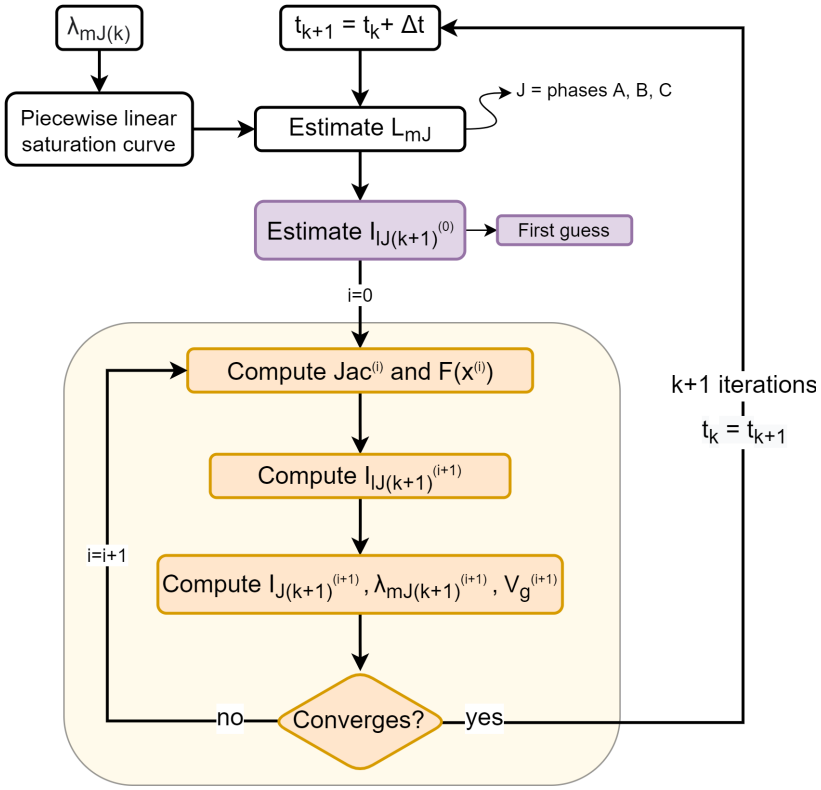

Figure 25: Programming flowchart for the Wye/Wye with primary directly grounded case. The yellow frame represents the Newton Method.

5.4.3 Wye/Delta connection with primary directly grounded

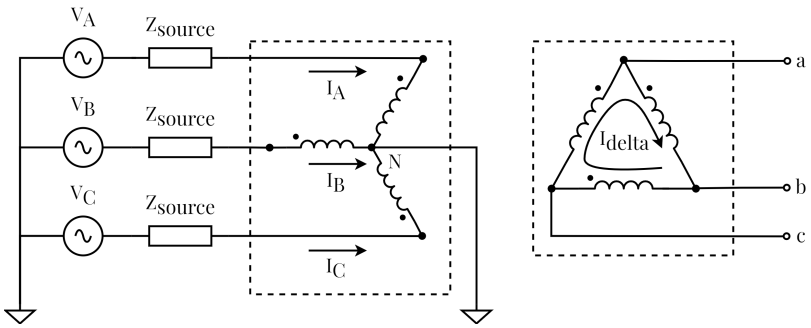

Figure 26: Three phase transformer in Wye/Delta connection with primary directly neutral grounded. The dashed squares mean that the three-phase transformer representation is simplified. The model is completed with Figure 22.

The delta loop in Figure 26 allows a current I_{delta} to flow in the secondary winding. This current,

excited from the primary side, causes the same voltage drop in all three secondary lines because R_2 and L_2 are of equal value in each phase (see Figure 27).

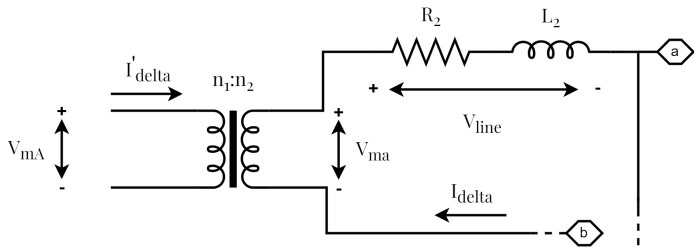

Figure 27: Delta current excited from the primary side (cropped view)

This idea deals to the following expressions:

$$3 \cdot V_{line} = V_{ma} + V_{mb} + V_{mc} \tag{37}$$

$$V_{line} = L_2 \cdot \frac{dI_{delta}}{dt} + R_2 \cdot I_{delta} = \frac{V_{ma} + V_{mb} + V_{mc}}{3} \tag{38}$$

For convenience, the same concept is applied moving the elements to the primary side, obtaining:

$$L_2^{'} \cdot \frac{dI_{delta}^{'}}{dt} + R_2^{'} \cdot I_{delta}^{'} = \frac{V_{mA} + V_{mB} + V_{mC}}{3} = \frac{\sum\limits_{J=A,B,C} \left(\frac{d\lambda_{mJ}}{dt} \right)}{3} \tag{39}$$

Now, because $I_{delta}^{'}$ is absorbing an "extra" current from the grid, the Equation 12, which was identical for cases 5.4.2 and 5.4.1, has to be updated:

$$I = I_l + I_r + I_{delta}^{'} \tag{40}$$

In consequence, a different (but similar to Equation 16) differential equation is obtained:

$$V - L \cdot \frac{dI_{delta}^{'}}{dt} - R \cdot I_{delta}^{'} = B \cdot \frac{dI_l}{dt} + C \cdot I_l \tag{41}$$

Whenever a variable is followed by the symbol $'$, it denotes that it is referred to the primary side

Now, applying KVL to the circuit in Figure 26:

$$\begin{cases} V_A - L \cdot \dfrac{dI'_{delta}}{dt} - R \cdot I'_{delta} = B_A \cdot \dfrac{dI_{lA}}{dt} + C \cdot I_{lA} \\ V_B - L \cdot \dfrac{dI'_{delta}}{dt} - R \cdot I'_{delta} = B_B \cdot \dfrac{dI_{lB}}{dt} + C \cdot I_{lB} \\ V_C - L \cdot \dfrac{dI'_{delta}}{dt} - R \cdot I'_{delta} = B_C \cdot \dfrac{dI_{lC}}{dt} + C \cdot I_{lC} \\ L'_2 \cdot \dfrac{dI'_{delta}}{dt} + R'_2 \cdot I'_{delta} = \dfrac{\sum\limits_{J=A,B,C} \left(\dfrac{d\lambda_{mJ}}{dt} \right)}{3} \end{cases} \tag{42}$$

This system has the same properties than in 5.4.2 (except because there is one extra variable and equation), and it can be solved in a very similar way using the Trapezoidal and Newton Method. The programming steps are represented in Figure 28, and the code is attached in Appendix B.

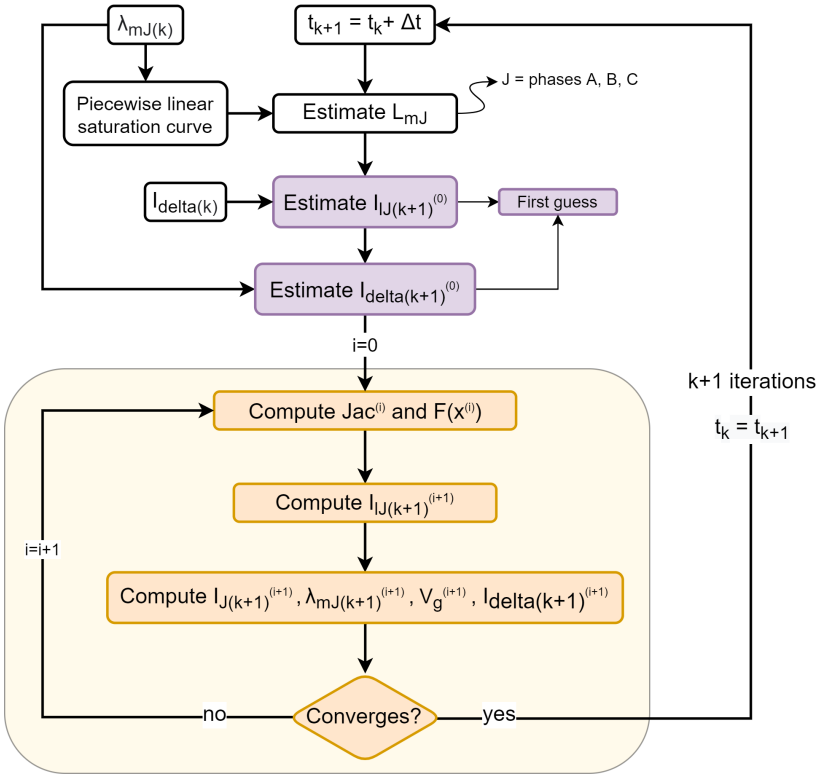

Figure 28: Programming flowchart for the Wye/Delta with primary directly grounded case. The yellow frame represents the Newton Method.

5.4.4 Wye/Delta connection with primary isolated

This last case is very similar to 5.4.2, but now the sum of currents $I_A + I_B + I_C$ needs to be null according to Kirchhoff's Current Law (see Figure 29).

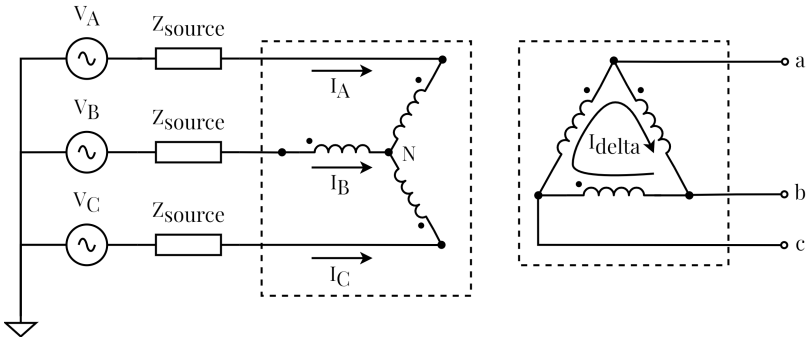

Figure 29: Three phase transformer connected in Wye/Delta with primary neutral isolated. The dashed squares mean that the three-phase transformer representation is simplified. The model is completed with Figure 22.

This means that one of the three line currents can be written in terms of the other two:

$$I_C = -I_A - I_B \tag{43}$$

Combining Equation 43 with Equations 40 and 11 for each phase:

$$I_{lC} = -I_{lA} - I_{lB} - 3 \cdot I'_{delta} - \sum_{J=A,B,C} \left(\frac{L_{mJ}}{R_m} \cdot \frac{dI_{lJ}}{dt} \right) \tag{44}$$

Now, applying KVL to the circuit in Figure 29:

$$\begin{cases} V_A - L \cdot \dfrac{dI'_{delta}}{dt} - R \cdot I'_{delta} = B_A \cdot \dfrac{dI_{lA}}{dt} + C \cdot I_{lA} \\ V_B - L \cdot \dfrac{dI'_{delta}}{dt} - R \cdot I'_{delta} = B_B \cdot \dfrac{dI_{lB}}{dt} + C \cdot I_{lB} \\ I_{lC} = -I_{lA} - I_{lB} - 3 \cdot I'_{delta} - \displaystyle\sum_{J=A,B,C} \left(\frac{L_{mJ}}{R_m} \cdot \frac{dI_{lJ}}{dt} \right) \\ L'_2 \cdot \dfrac{dI'_{delta}}{dt} + R'_2 \cdot I'_{delta} = \dfrac{\displaystyle\sum_{J=A,B,C} \left(\frac{d\lambda_{mJ}}{dt} \right)}{3} \end{cases} \tag{45}$$

The programming steps are represented in Figure 30, which are almost identical to the ones in Figure 28.

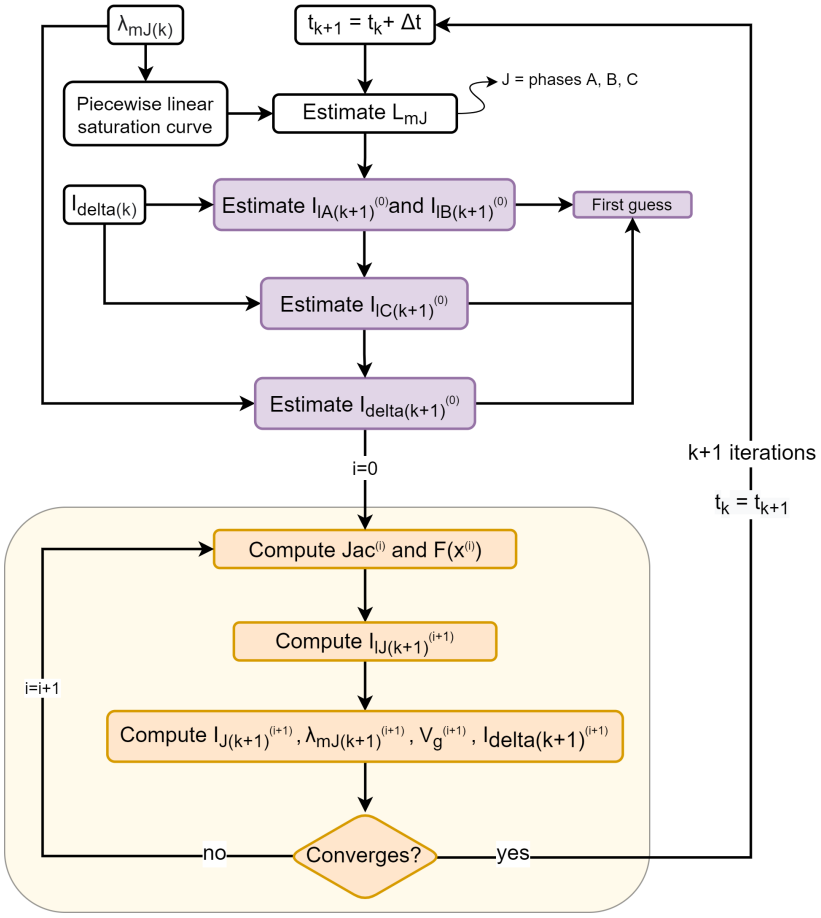

Figure 30: Programming flowchart for the Wye/Delta with primary isolated case. The yellow frame represents the Newton Method.

6 Model Implementation and Verification

The final step in the process is to verify that the designed model is consistent with conventional software dedicated to study power system transients such as Matlab and PSCAD. This is the only way to verify that the model is correct, as there are no measurements available. PSCAD offers a very restricted license for free, but enough for verification, and Lund University grants full access to the Matlab license and the Simscape Electrical plugin.

The reader is reminded that the outcome of the last chapter is four different algorithms, one for each connection type in Table 2. The implemented code is available in the Github repository [25]. In this chapter, all four connection types will be compared one by one against the just mentioned software.

This section can be divided in three subsections: Firstly, a reference study case is described and prepared for simulation. Secondly, the models used in PSCAD and Matlab are indicated. Finally, all the results are compared qualitatively.

6.1 Study Case

In order to do the simulation under realistic conditions, a transformer is selected from the research paper in [26], which had sufficient information regarding saturation conditions. However, some parameters were forced to a different value to fit other literature suggestions and the requirements of all three simulation software. Also because all connection types are to be compared, the same test report was used for each of them. The final values are summarised in Tables 3 and 4.

Each software demands some kind of conversion of the data provided in Tables 3 and 4 in order to use them as an input in the program interface. Appendix C: Transformer Data Conversion lists the equations required to determine the values of the individual elements in the three-phase models described in Chapter 5 from a typical test report and that are substantiated in [27].

Transformer properties	Value
Rated Power	2.1 MVA
Rated Voltage	11kV/690V
Rated Current	110A/1757A
Configuration	Ygy, Ygd, Yy, Yd
Leakage reactance	0.0267 p.u.
No load losses	0.00146 p.u.
Copper losses	0.003 p.u.
Air core reactance	0.4 p.u.
Knee voltage	1.15 p.u.
Magnetizing current	0.3 %
Residual flux	0

Table 3: Reference transformer characteristics [26](modified)

Equivalent network parameter	Value
Equivalent resistance	0 Ω
Equivalent inductance	0.022 H

Table 4: Network thevenin equivalent resistance and inductance [26](modified)

6.2 PSCAD Model

One of the main restrictions in the design of the PSCAD model is the open circuit branches, which are always needed at the secondary of the transformers (for energization at no load) and sometimes in the ground connection of the primary winding depending on the connection type. In PSCAD, the open circuit branches have to be modelled with a large resistance to ground, but sometimes it can produce convergence problems. This occurs for the connections with primary ungrounded, where the greatest resistance to ground that converges is 1000 ohm. Surprisingly, this phenomenon also happens with the proposed algorithm in Chapter 5.4.2.

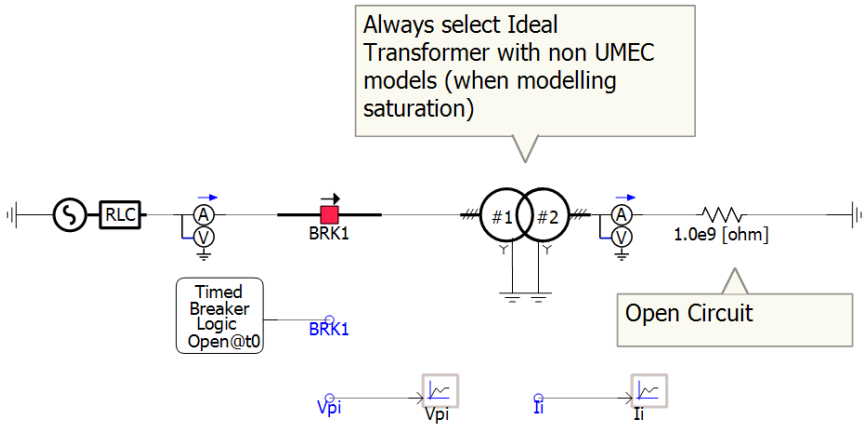

Figure 31: PSCAD model for a Wye/Wye connection with primary (and secondary) grounded

Additionally, PSCAD saturation properties include an additional parameter named *"Inrush Decay Time Constant"* that artificially damps the current. This is a very different way to simulate the damping, as Matlab and the proposed algorithm only take into account the losses in the system. Therefore, even if PSCAD suggest some realistic values for this parameter, the current decay is not expected to be identical in the other alternatives.

To match the same conditions in all three softwares, the circuit breaker "BRK1" has been designed to close at the exact time the phase A voltage crosses zero as it ascends. This also applies for the circuit breaker "Switchgear" in Figure 32.

6.3 Matlab Simscape Electrical Model

The most significant difference with respect to PSCAD is the way saturation is modelled. Instead of using dedicated parameters such as the *Knee point* or the *Air core reactance* (see Figure 14), arbitrary points from the saturation curve are manually added as: $(current_1, flux_1, i_2, f_2, ..., i_n, f_n)$, where i_i and f_i are the values of any point (i_i, f_i) in the saturation curve of the transformer.

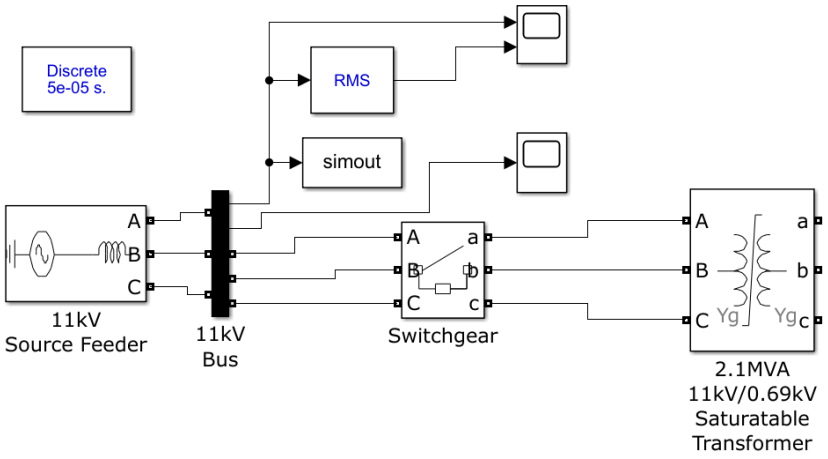

Figure 32: Matlab model for a Wye/Wye connection with primary (and secondary) grounded

6.4 Comparison of Results

In this section the simulation results obtained in Python during the energization of the reference transformer described in Chapter 6.1 are compared with respect to the models in Matlab and PSCAD in every connection type mentioned in Table 3.

The main disadvantage of the designed solution is that it is less computationally efficient than its competitors (takes more computation time), and it requires more precision to achieve the same or very similar result. It is a matter of time that a simulation based on numerical method algorithms looses accuracy. However, this is not very visible in Matlab and PSCAD if compared to the situation depicted in Figure 33. The consequence is that the further in time, the less reliable the obtained results are.

That being said, deciding on which step size to use is a compromise between precision and computation time, although experimental results suggest using a step size no greater than $5 \cdot 10^{-6}$ seconds. This is one order of magnitude more costly than the default settings in both Matlab and PSCAD, and the reason might be behind the mathematical algorithms they use to solve differential equations, which have been optimized to be efficient and precise for that specific purpose. Still, the optimal step-size is specific for each distinct situation and should not be generalized.

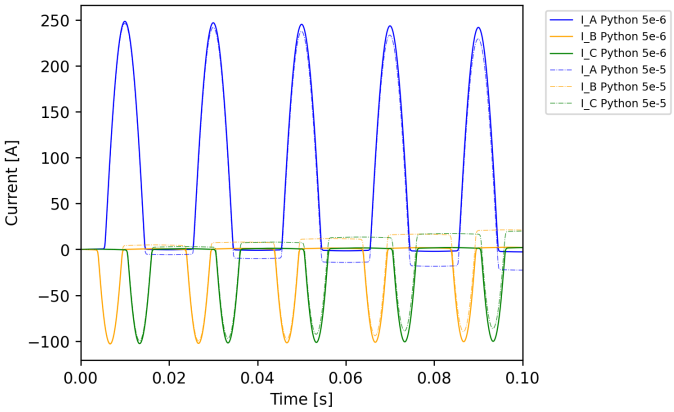

Figure 33: Effect of using different step sizes under the same conditions: the solid line represents a simulation with an accuracy of $5 \cdot 10^{-6}$ seconds, while the dashed line corresponds to an accuracy of $5 \cdot 10^{-5}$ seconds that make the results drift away with time.

6.4.1 Wye/Wye connection with primary directly grounded

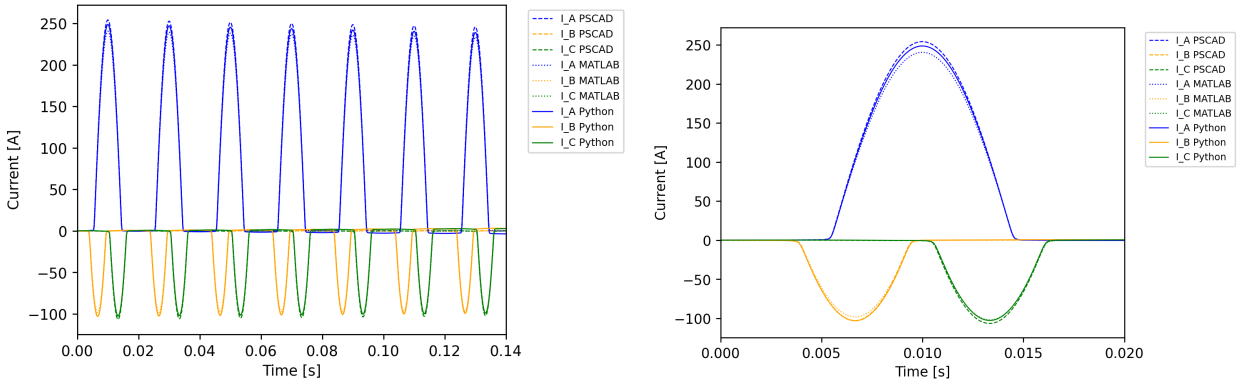

(a) **(b)**

Figure 34: Comparisson of results for Wye/Wye connection with primary directly grounded. a) Simulation of 0.14 seconds. b) Simulation of 0.02 seconds or one cycle.

What is surprising of this particular case is that phases B and C follow exactly the PSCAD and Matlab solution respectively. As this situation is not repeated in later comparisons, it can be considered as a casual coincidence.

6.4.2 Wye/Wye connection with primary isolated

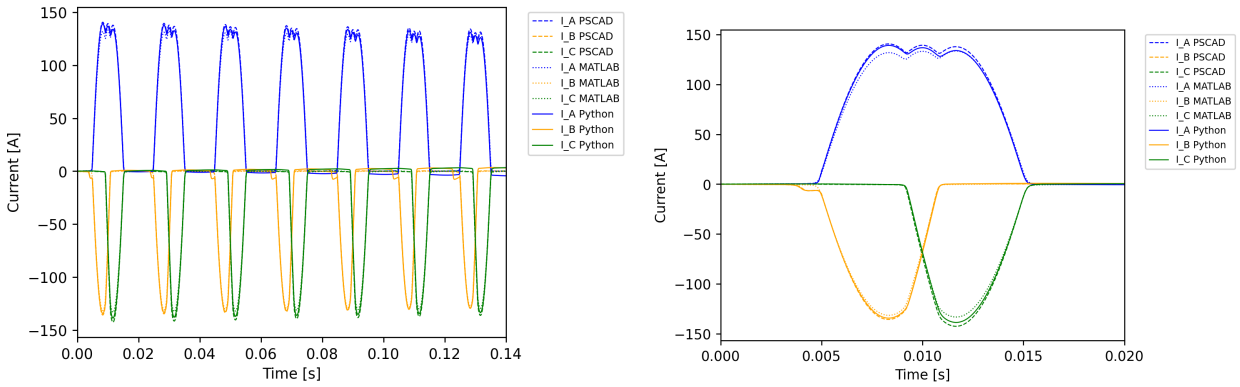

(a) **(b)**

Figure 35: Comparisson of results for Wye/Wye connection with primary isolated. a) Simulation of 0.14 seconds. b) Simulation of 0.02 seconds or one cycle.

One characteristic of these waveforms that is worth commentating is the high presence of harmonics that could not find a path to ground in the primary winding. Additionally, the small bump that appears in phase B at the start of every cycle, which can seem like a possible error at first, is consistent with the PSCAD solution.

6.4.3 Wye/Delta connection with primary directly grounded

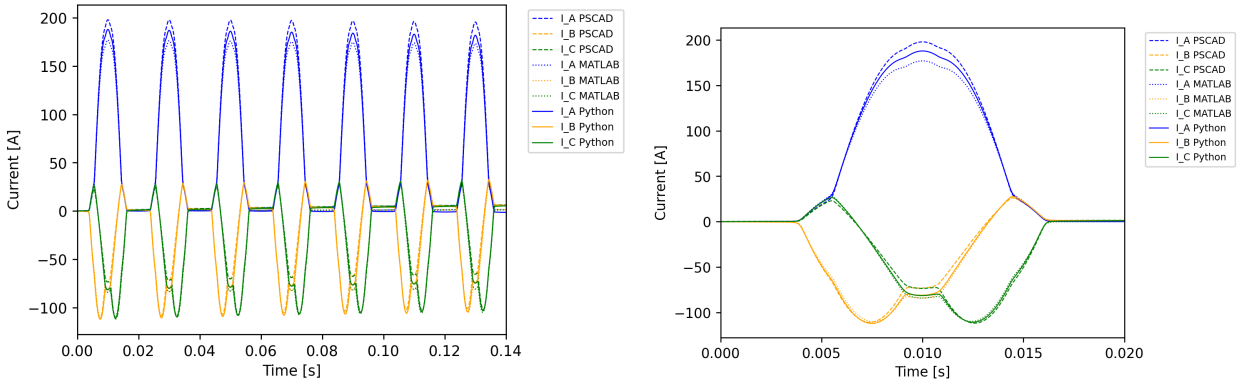

(a) **(b)**

Figure 36: Comparisson of results for Wye/Delta connection with primary directly grounded. a) Simulation of 0.14 seconds. b) Simulation of 0.02 seconds or one cycle.

6.4.4 Wye/Delta connection with primary isolated

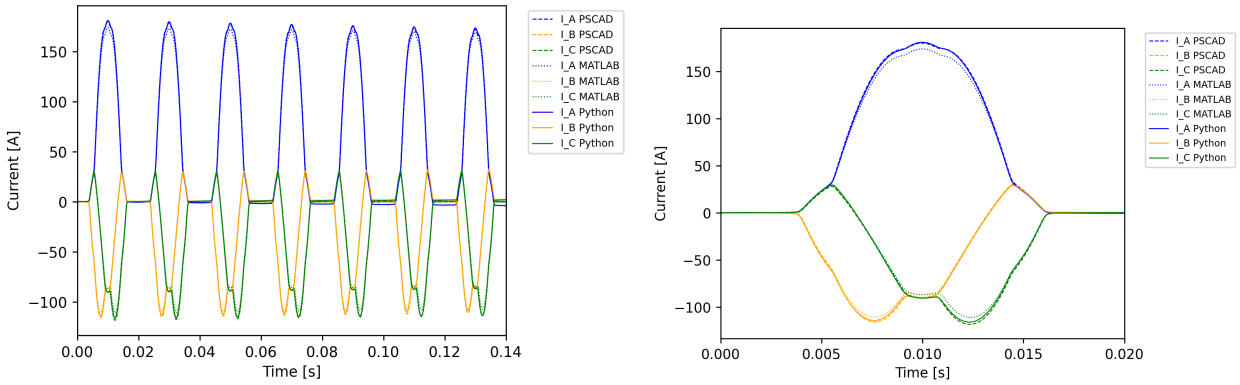

(a) **(b)**

Figure 37: Comparisson of results for Wye/Delta connection with primary isolated. a) Simulation of 0.14 seconds. b) Simulation of 0.02 seconds or one cycle.

In this last case, the obtained solution is clearly more similar to the PSCAD reference. This is surprising because the isolation of the primary winding has been modelled in a different way (see Chapters 6.2 and 5.4.4).

6.5 Verification summary and comments

In all cases, it is successfully demonstrated that the achieved solution is always between the PSCAD and Matlab reference. It is interesting to notice that, whenever the secondary winding is connected in delta, the simulated inrush current is smaller in magnitude if compared with the case when the secondary is wye connected. The same principle applies for the connection to ground of the primary winding: if it is isolated, the resultant current is smaller if compared to the grounded case. This is directly related to the zero sequence impedance: Delta winding has infinite zero sequence impedance and primary is directly grounded to the smallest one.

It is also of interest to show the comparison concerning the regular operation of the transformer and appreciate the inrush current effect. As seen in Figure 38, the inrush current for the Wye/Wye connection with primary directly grounded reaches about 1.5 times the peak of current during regular operation of the transformer. The impact could have been considerably more severe if the maximum residual flux had been considered.

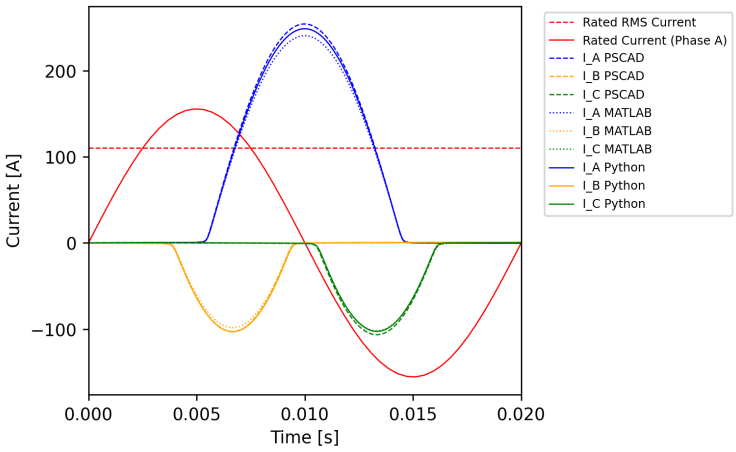

Figure 38: Comparison of results for Wye/Wye connection with primary directly grounded, including regular operation of transformer

Note: in Figure 38, the rated current is shifted horizontally with respect to its true position.

This page is intentionally left blank

7 Grid Analysis and Power Quality

In many utilities, the principal hazard associated with transformer energization is power quality, although in extreme cases where the electrical instruments are old and poorly maintained it can cause critical damage to transformers. If supply quality issues are not addressed, this may result in fines and compensation payouts which will have an impact on the company's finances, operations, and regulatory integrity [28].

This section is meant to analyse the impact of transformer energization in the grid, focusing on the voltage dip, while other consequences such as misoperation of protection relays or resonant overvoltages are only briefly discussed. As it has been explained in Chapter 1, the main tool used for this purpose is PSS/E. In contrast with EMTP-like programs, PSS/E is based on phasor representation of voltages and currents, assumes only the fundamental frequency and disregards all harmonics. Its applications are mainly reduced to power flow calculations with symmetric conditions, although some fault analysis may include asymmetry. Therefore, this chapter is also about the connection between "Grid analysis" and "Simulation" in Figure 5 using the PSS/E built-in Python API [29].

7.1 Harmonics

One of the main characteristics of inrush currents is its rich harmonic content. It is important to evaluate it properly as the design of protection relays and the analysis of resonant overvoltages depend on it. In most contributions, the harmonic analysis is performed by looking at the variation of its harmonic content with time (see Figure 39), which changes a lot during the inrush current decay. Transformer protections should distinguish a fault event from the differential currents that may result from its energization, and the simplest criteria uses the ratio between the magnitude of the second harmonic and that of the fundamental frequency component. However, this method is becoming more difficult to implement as modern transformers produce a lower magnitude of the second harmonic component after a switching event [30]. When the inrush current interacts with the resonant frequencies of the system, it may result in long-duration resonant temporary overvoltages, especially during the restoration of a black-out or in HVDC[8] and long cable systems [5], but this undesired situations are out of scope of this report.

[8] High-voltage Direct Current

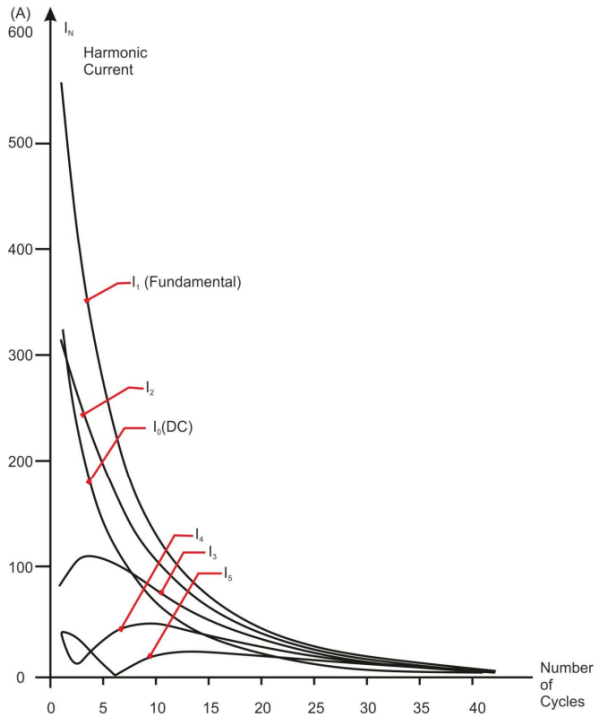

Figure 39: Harmonic component of inrush current [5]

For future applications (see Chapter 7.3.2) it is useful to calculate the harmonic content of the inrush current waveform, which has been done applying the Discrete Fourier Transform (DFT) with the aid of a Python library [31]. Because the harmonic spectrum varies during time, it has been decided to apply the DFT over the two first cycles of the simulation to be representative of the moment after the switch is closed. An example is available in Appendix A, Figure 51b.

7.2 Voltage Dip Requirements

The inrush current must be supplied by the system sources, and flows through the network impedance to the transformer being energized, causing a voltage drop across the network impedance with increasing effect towards the transformer. The voltage dip recovers as the inrush current decays, which can take from seconds to minutes and depends mainly on the losses in the circuit. This requires special considerations when there are sensitive loads in the system such as adjustable-speed drives and programmable logic-based process control in paper, mining and electronic chip manufacturing plants [30].

E.ON has the responsibility to ensure that power quality is maintained when transformers are energized. From all the possible ways that magnetizing inrush currents can impact the grid, the focus (according to E.ON policies and their future use of this tool) should be the voltage dip produced at the energizing and nearby buses. The Energy Market Inspectorate has classified voltage dips according to [32], shown in Figures 40 and 41, where it must not occur any short-term voltage drop with such residual voltage and such duration as shown in the area indicated as “C”. Additionally, the network owner is obliged to remedy short-term voltage reductions within area “B”

to the extent that the measures are reasonable concerning the inconveniences caused to electricity users associated with the short-term voltage reductions. In practice, electric operators decide how much they approximate the regulatory limits to ensure that they will not have to face any penalties.

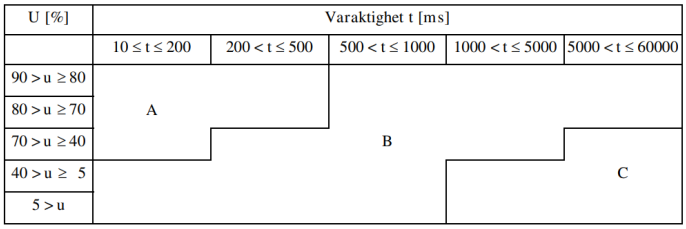

Figure 40: Voltage dip classification for nominal voltages up to and including 45 kV [32]

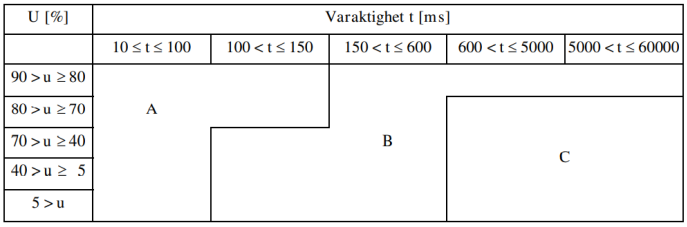

Figure 41: Voltage dip classification for nominal voltages above 45 kV [32]

Therefore, E.ON is interested in having a reasonably accurate model to predict if any bus will be within sensible limits providing that a transformer has been energized. Additionally, E.ON may have special commitments with consumers that constrain even more the requirements, such as a voltage drop allowance of up to 3-5%.

7.3 Impact of Voltage Dip on the Surrounding Grid

The prediction of voltage dip at different points in the grid due to transformer energization can be quite challenging, especially if it has to be carried out using PSS/E, which is of a very different nature than the precise time simulations explained in previous sections. The main difficulties can be summarised in:

1. Obtaining a positive sequence magnitude of the desired variables, since one of the main characteristics of inrush currents is their asymmetrical waveforms and the presence of harmonics that PSS/E cannot handle.

2. Finding the proper techniques to be used in PSS/E that can be representative for the scenario that will occur in the real situation, and the limitations of proving its accuracy. For solving this issue, two alternative methods have been proposed, without deciding on any of them neither measuring its preciseness.

7.3.1 Strategy 1: Using a Regulated Voltage Source

The first and easiest strategy comes from the idea of replicating in PSS/E the simulated voltage dip curve at the energizing bus. To implement this strategy, there are two possibilities:

- Obtaining a positive equivalent voltage magnitude V_1 from the varying phase RMS values V_a, V_b and V_c at the energizing bus employing Fortescue's Theorem:

$$\begin{pmatrix} V_0 \\ V_1 \\ V_2 \end{pmatrix} = \frac{1}{3} \cdot \begin{pmatrix} 1 & 1 & 1 \\ 1 & a & a^2 \\ 1 & a^2 & a \end{pmatrix} \cdot \begin{pmatrix} V_a \\ V_b \\ V_c \end{pmatrix} \tag{46}$$

  Where $a = 1\angle 120°$. In Figures 42a and 42b are shown an example of the sequence voltages calculated from a certain RMS phase voltage curve using Equation 46.

- Using directly the most severe phase RMS voltage drop, as in [5] is mentioned that the most affected phase should be used as the basis for quantifying the voltage dip event.

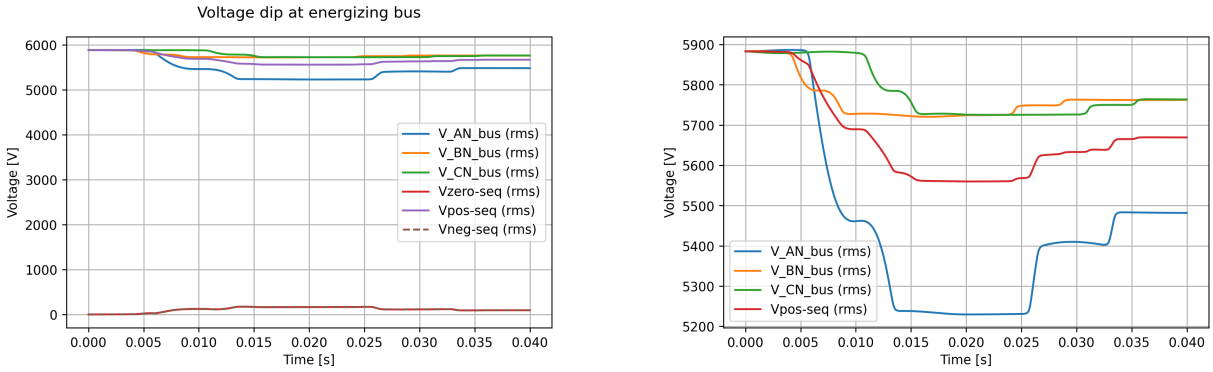

(a) Phase and sequence voltages

(b) Figure 42a in more detail

Figure 42: Sequence voltage calculation example

For both options, their magnitude values in p.u. are used as the input of an artificial regulated voltage source with zero series impedance and the voltage is observed at other nearby buses (see example in Figure 52a). The voltage angle at the energizing bus is considered as another variable of the power flow calculation. Regarding the power flow settings, shunts and taps adjustments are not considered because their response times are higher than those taken into account in the simulation. In Figure 43 a flowchart of the process is shown, which is repeated at every time step.

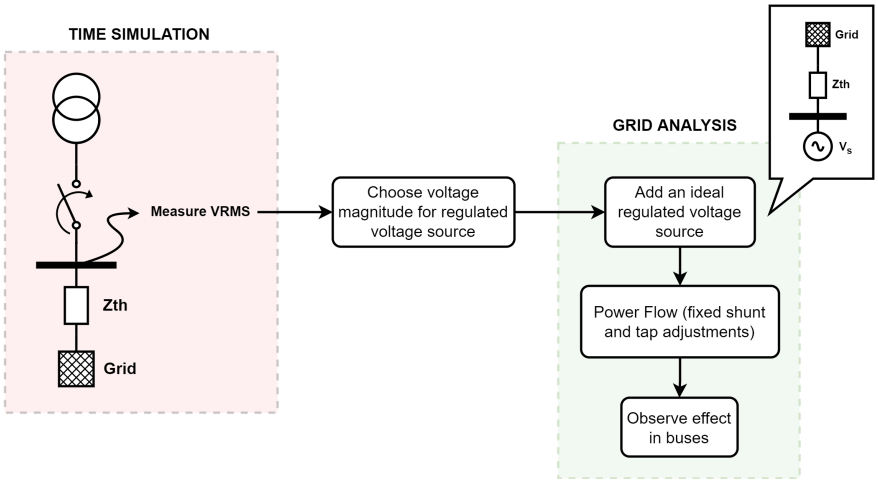

Figure 43: Flowchart of strategy 1, repeated at every time step

7.3.2 Strategy 2: Using a Symmetric Load

This method is related to the current waveform instead of the RMS voltage drop curve. The goal is to find an equivalent symmetrical current absorbed by a load that will be artificially placed at the energizing bus. There is the possibility to choose which current magnitude to use from the following options:

- Positive RMS current magnitude, obtained in a similar way as in Equation 46.
- Phase RMS current magnitude. It will be automatically selected the most extreme phase in this and following cases.
- Just considering the current highest peak value.
- The fundamental frequency magnitude (FF) obtained from the harmonic spectrum of the inrush current waveform.
- Adding the DC component to the fundamental. This is calculated as:

$$\sqrt{I_0^2 + I_1^2} \tag{47}$$

- Adding all the harmonics as:

$$\sqrt{I_0^2 + I_1^2 + I_2^2 + ... + I_n^2} \tag{48}$$

When it is decided which current magnitude to use, it should be computed the three-phase load power P and Q using the known voltage magnitude and angle at the energizing bus.

$$S = P + Qj = \sqrt{3} \cdot V\angle\phi_v \cdot I\angle\phi_i{}^* \tag{49}$$

Where $I\angle\phi_i$ is assumed to be 90^{o} lagging with respect to $V\angle\phi_v$ because the magnetizing current is absorbed by the magnetizing inductance, meaning it is reactive with respect to its exciting voltage.

$$\phi_i = \phi_v - 90^{\circ} \tag{50}$$

As a consequence of the above hypothesis, the load has no active power component. Which load to add cannot be determined on its own, since adding a load to the system will inevitably alter the voltage profile. Therefore, it is required to do an iterative process until all variables converge, otherwise the resultant current will be different than the desired value. During the observation of the grid after the load is inserted in the model, the voltage at the energizing bus is set free, and the power flow is performed in the same way as in the previous strategy, with fixed shunts and taps adjustments. In Figure 44 a flowchart of the process is shown.

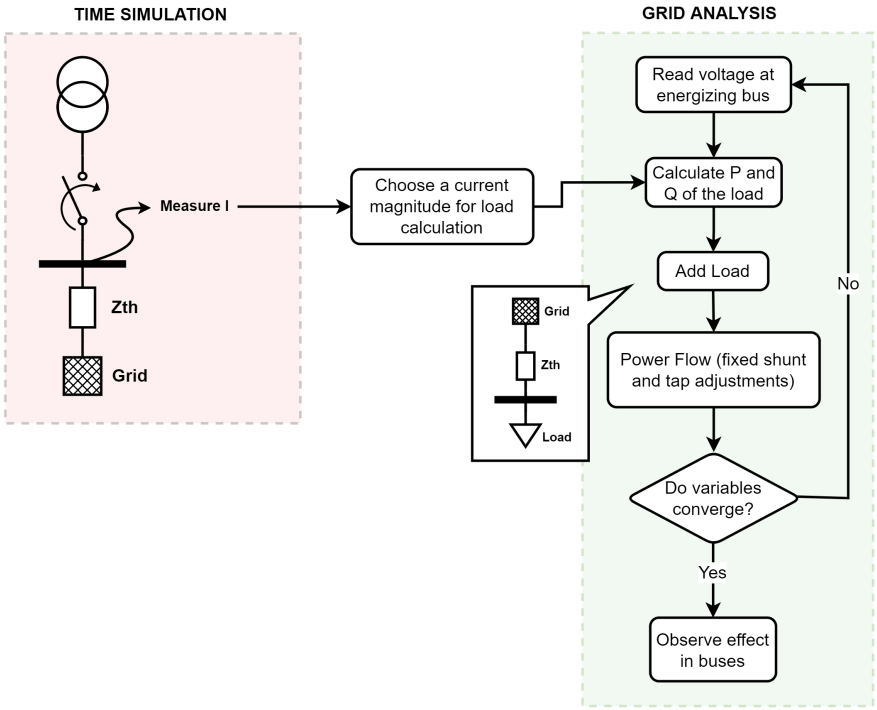

Figure 44: Flowchart of strategy 2

7.3.3 Example Case: Comparison of Strategies

To compare the two methods proposed, E.ON provided access to a small part of their grid model in PSS/E. This area corresponds to a medium voltage network of 35 buses of the south part of Öland ranging from 130 kV to 11 kV. It was tested the hypothetical energization of the farthest transformer from the 130 kV node (marked in green in Figure 45), with default saturation properties assumed (most severe case). The 4 MVA 55/11.5 kV transformer is Wye/Wye connected with primary directly grounded. The voltage dip was observed at all the proximate buses within two levels (from grandparent nodes to energizing bus) with both strategies and compared afterwards.

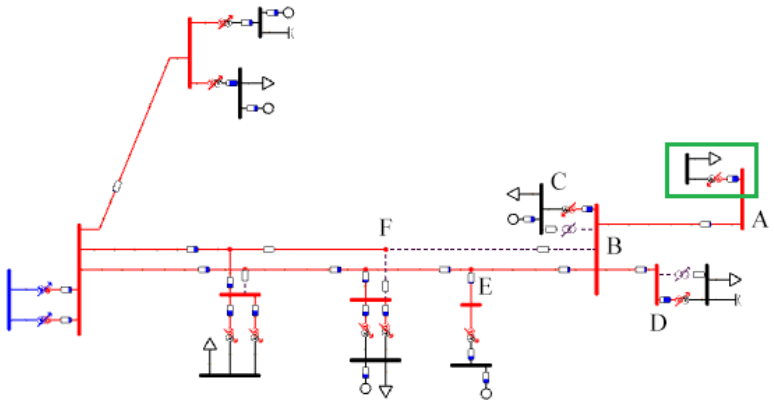

Figure 45: South Öland medium voltage network. 135 kV (blue) - 55 kV (red) - 11kV (black). Squared in green, the location of the transformer that is going to be energized.

From Figure 46 it is possible to say that the results can differ a lot from one method to another. Moreover, not all methods will provide a readable solution as sometimes, depending on the case, it may not converge. This actually happened with the peak value option at this particular example. The reason might be that its very high current magnitude (the highest from all options) causes a voltage reduction that PSS/E cannot manage.

In all tested scenarios, the current approach seems to cause more voltage reduction than the alternative method.

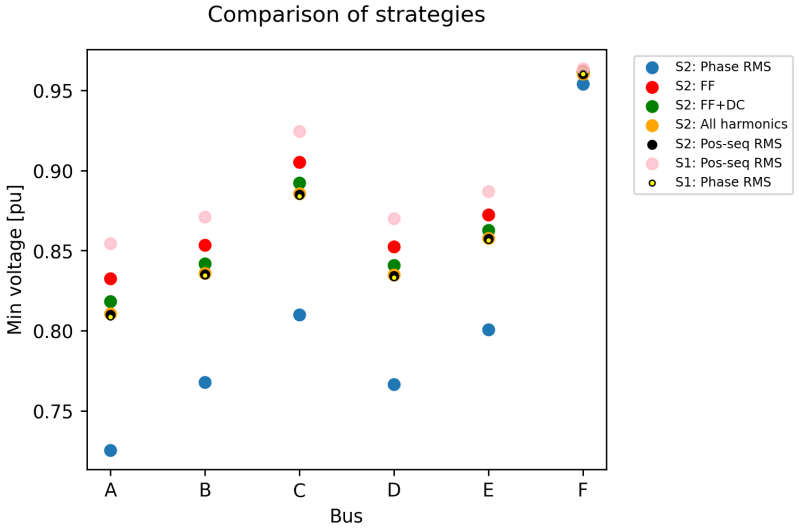

Figure 46: Observed minimum voltage at nearby buses according to different strategies. In the x-axis, the first bus corresponds to the energizing bus, and the more to the right, the farther away that bus is. In the legend, "S1" is the abbreviation for Strategy 1, and "S2" the abbreviation for Strategy 2.

Even if it is hard to extract some conclusions from only this information, it is possible to say that the phase RMS option of strategy 2 together with the peak value (which did not converge) is probably overestimating the voltage reduction, and that the positive RMS and fundamental frequency option represent a more realistic lower and superior limit of possible outcomes for strategy 2.

It is interesting to note that the voltage dip estimated by the two strategies almost coincides on three occasions for all buses considered:

- Strategy 1 - Phase voltage RMS
- Strategy 2 - Adding all harmonics to the fundamental current magnitude
- Strategy 2 - Positive sequence RMS current

The listed sub-strategies are considered more trustful not only because of the casual correlation between them, but also because they produce results consistent with literature measurements of a similar network, where the most severe voltage dips reach 10% to 15% according to Figure 47. The pre-energization voltage at bus A (the energizing bus) is 0.91 p.u. Therefore, the estimated voltage dip is roughly 10%, which is within the expected values for a severe energization.

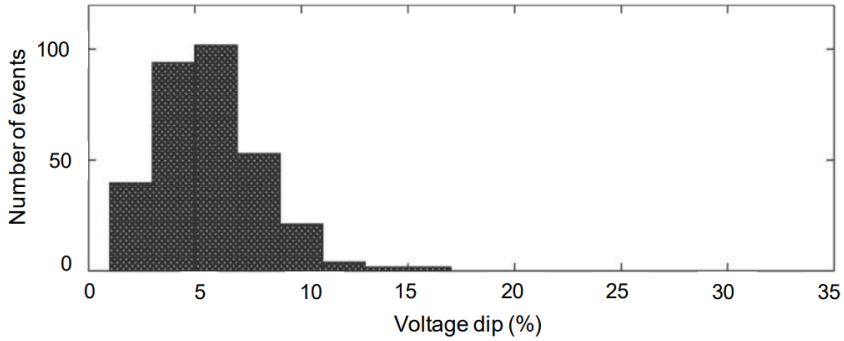

Figure 47: Frequency of RMS voltage dip magnitudes events measured at a 11 kV distribution network [11].

Refer to Chapter 8.2 for more details in a practical application using the developed tool.

8 Interactive Tool for Energizing Study

This Chapter focuses on showing what the interactive tool that will be used by the employees at E.ON for transformer energizing studies looks like from a user perspective.

Regarding the code, it will only be mentioned the one tool that was required to build the GUI in a Python environment, and that saved a huge amount of programming time due to its faculty to create pop-up windows and interact with the user: Tkinter, the standard Python interface [33].

The last section of this chapter (8.2) shows how any user of the tool could operate in a practical application.

8.1 Graphical User Interface

When the user runs the program, it first asks to choose a *sav* file where the network data is stored and recognised by PSS/E. This is a mandatory step as later on it will be required as input data and to estimate the impact of inrush current in the grid. Then, one of the two following methods needs to be selected:

- Manually introduce all transformer properties needed to perform the energization simulation.
- Use rated transformer properties from a specific transformer in the network data file, and complete them with additional manual parameters not represented in PSS/E (saturation, equivalent network...).

After making the decision, the program will show one of the following windows:

If the user does not have any information regarding the saturation characteristics of the transformer that is to be energized, a button has been designed to automatically use default values of *air core reactance*, *knee voltage*, and *residual flux*. These values are summarize in Table 5 and justified in Chapters 4.2 and 5.2.

Parameter	Default value
Knee point	1.15 p.u.
Air-core reactance	2· leakage reactance p.u.
Residual flux	0.8 p.u.

Table 5: Default saturation values

If any of the required information is not entered or admitted, a warning message will appear and the simulation will be aborted immediately.

The time simulation has also some settings that can be changed by the user, such as simulation time, step size, data resolution, what energization voltage to use, as well as grid analysis strategy. Because some of this concepts can be hard to define in one word, an informative box appears when the mouse hovers above a variable during some time.

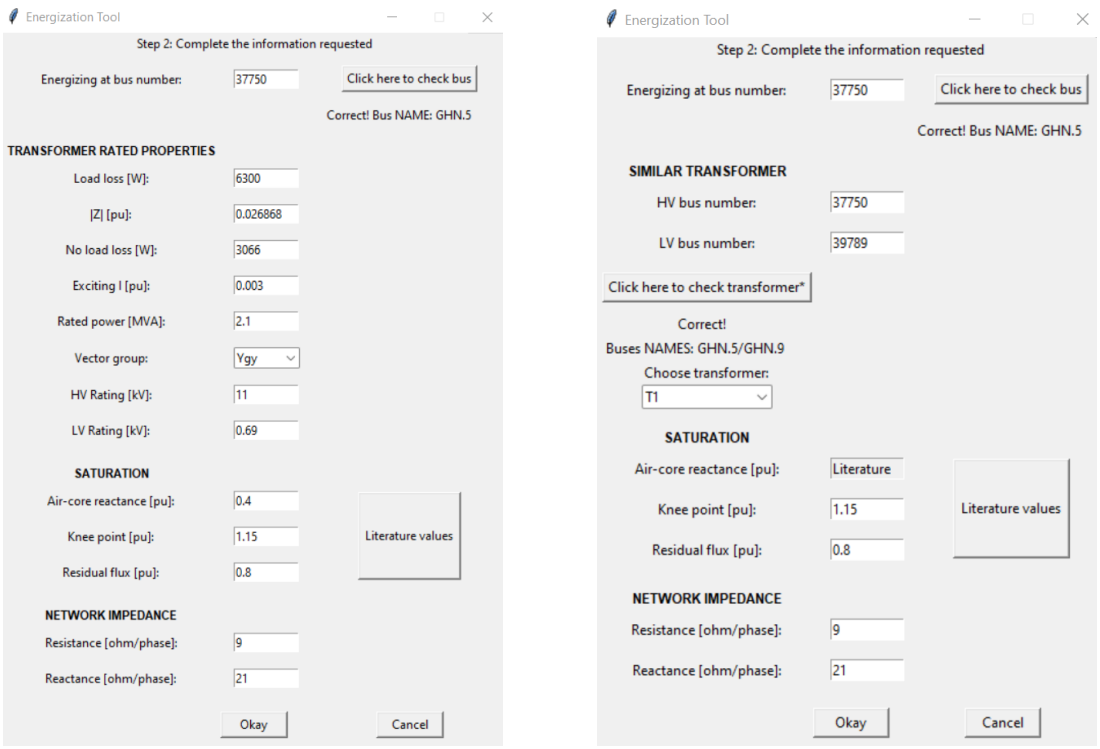

(a) Manual input **(b)** PSS/E transformer

Figure 48: Transformer data required by the program depending on the format selection

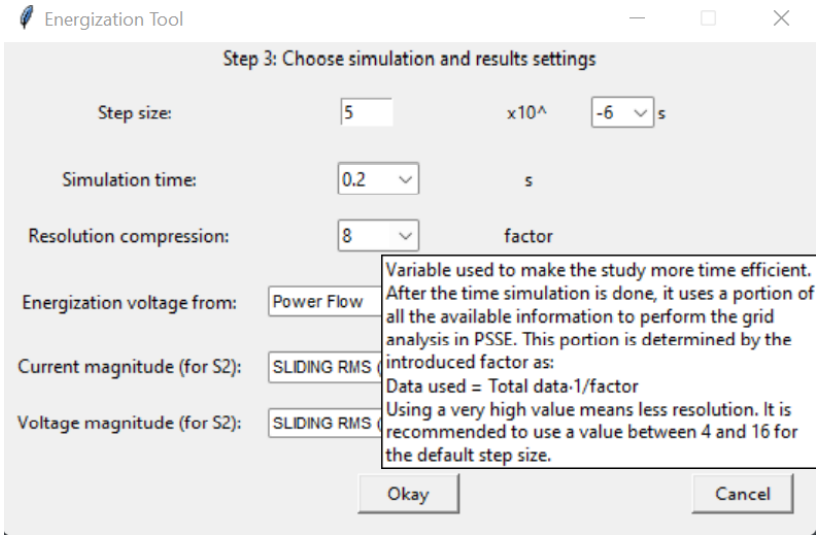

Figure 49: Simulation settings and informative box for "Resolution compression factor"

From all of these variables, "Energization voltage from" is worth explaining in more detail. Usually, in energization studies, the transformer is excited by the rated voltage of the network feeding the primary winding. However, it is also interesting to analyse the inrush current effect at different voltage levels. Moreover, the rated voltage at the energizing bus may differ from the rated voltage of the transformer. To take this into account, the user can choose to perform time simulations at

different voltages.

After all the input information is completed, the time-simulation starts. When finished, it returns a huge amount of data because the time step is, at least, of the order of microseconds. As an example, a simulation of one second with an accuracy of $1 \cdot 10^{-6}s$ will return 1 million data points for each variable under study (fluxes, voltages, currents, etc...). To give some perspective, the maximum number of rows and columns in an excel file are respectively 1,048,576 and 16,384. Therefore, if this data is going to be processed afterwards, it is better to *compress* it. That's the purpose of the variable "Resolution compression" in Figure 49.

With the compressed data, the grid analysis is done in PSS/E calling plenty of functions from the Python API [29] to achieve the objectives discussed in Chapter 7.

Only when all the tasks are finished, result plots are generated and automatically stored in a user's folder. These plots show different kinds of information:

- The inrush current waveforms, RMS (line and phase) voltage drop and RMS phase currents at the energizing bus. This is exported directly from the compressed time-simulation data. For the inrush current, an example is found in Figure 51a, and for the RMS phase current, see Figure 50a.
- Some variables are processed to obtain interesting information such as the harmonic spectrum of the inrush current (Figure 51b), the expected time for inrush decay (see Figure 50b), or the voltage dip comparison with respect to the grid regulations (Figure 50d).
- Finally, and as a result of the grid analysis, the impact of transformer energization in the grid is shown according to the strategies previously discussed. Some examples are found in Figures 50c, 52a and 52b.

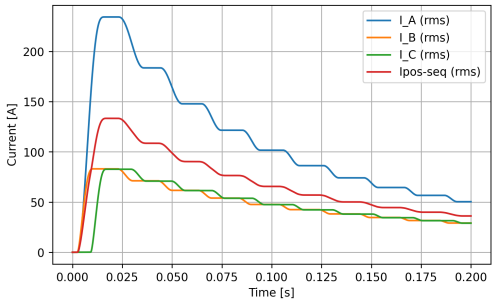

(a) RMS phase current

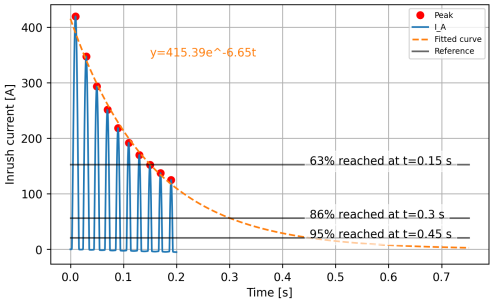

(b) Estimation of inrush decay

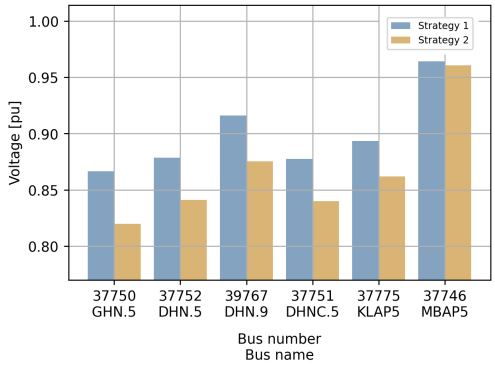

(c) Comparison of strategies 1 and 2

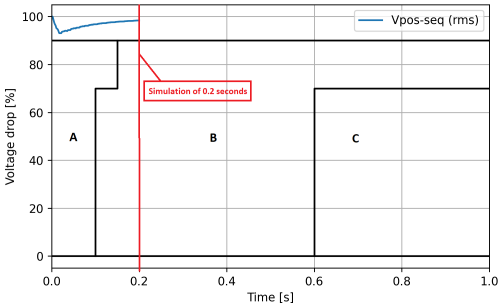

(d) Comparison with grid requirements

Figure 50: Tool output examples

8.2 Example of Use

Let's suppose that E.ON engineers are interested in determining the largest possible transformer that they can install at the same location as in the example case (see Figure 45) so that its energization will not cause severe voltage dips. The actual transformer rated size is 4MVA, which according to the energization simulation results with custom settings (see Figures 51 and 52), will cause a voltage dip of approximately 10% at the energizing bus, just as it was mentioned in Chapter 7.3.3.

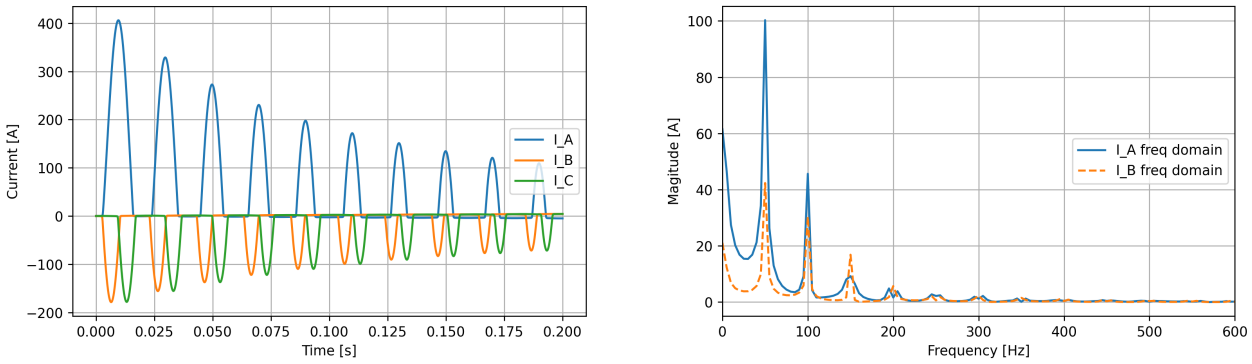

(a) **(b)**

Figure 51: Inrush current (a) and its harmonic spectrum (b) during the energization of a 4 MVA 55Yg/11.5y kV transformer in Öland's medium voltage network.

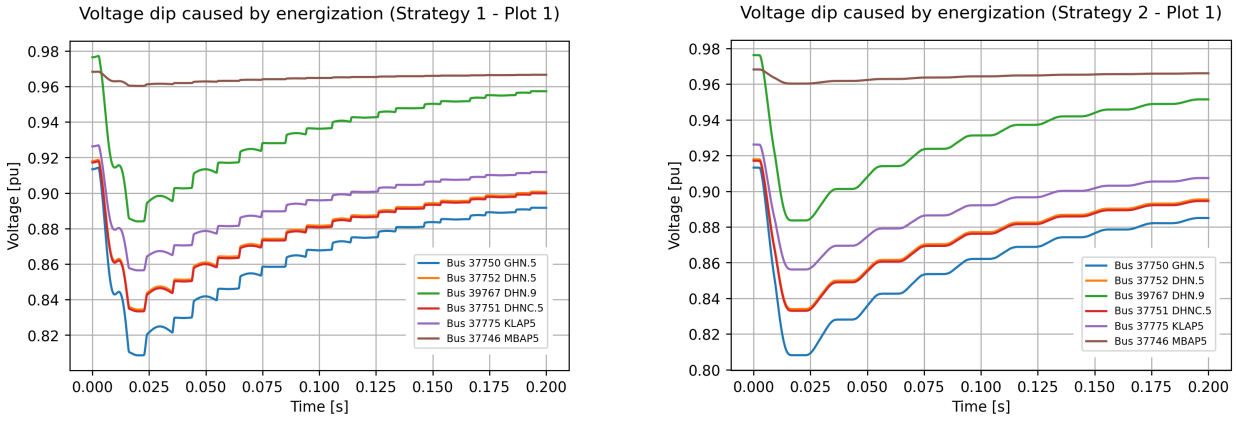

(a) **(b)**

Figure 52: Observed voltage dip at nearby buses using two different strategies: a) Strategy 1 - Phase RMS voltage. b) Strategy 2 - Positive sequence RMS current.

The bus numbers appearing in Figure 52 are not consistent with the letters in Figure 46 because they were simplified for better readability. The relation between both is presented in Table 6.

Bus number	Bus letter
37750	A
37752	B
39767	C
37751	D
37775	E
37746	F

Table 6: Relationship between bus number and letters

Now, repeating the same simulation multiple times but raising the transformer size each moment, it is possible to estimate the effect that this increment can have on the energizing bus and the surrounding area. Figure 53 compares voltage values versus transformer size:

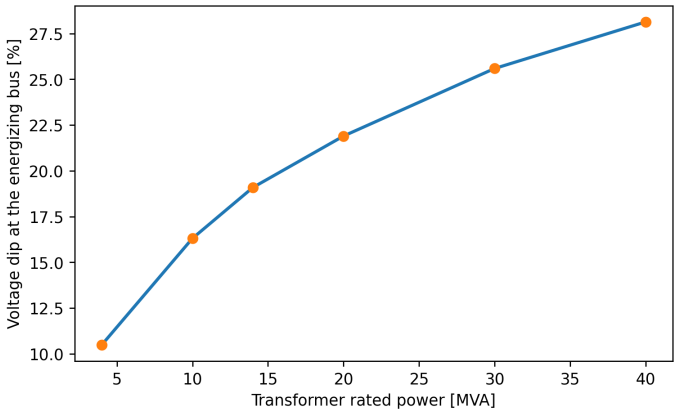

(a) Simulated voltage dip at the energizing bus

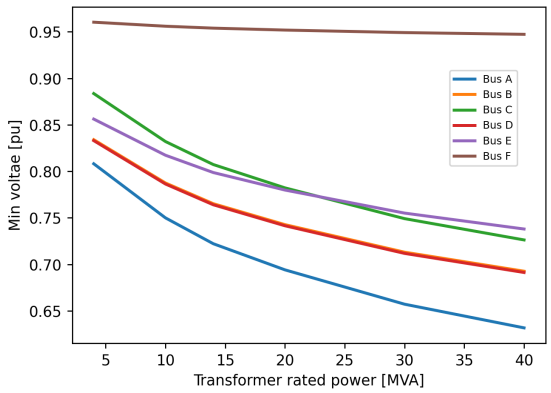

(b) Simulated voltage dip at different buses - S1

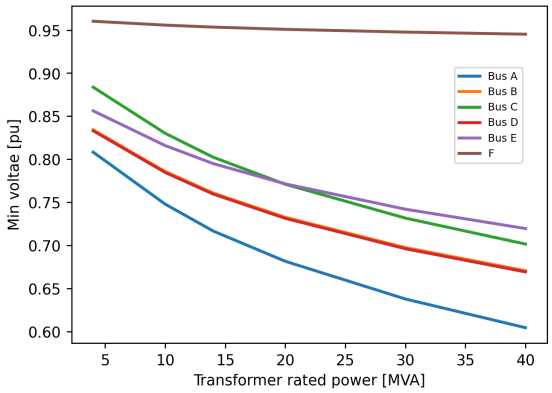

(c) Simulated voltage dip at different buses - S2

Figure 53: Simulated transformer energization impact on voltage when varying the transformer size. Note how the curves follow an exponential shape.

With this information, the user can decide how much it is possible to increase the transformer size given certain limits imposed by regulatory organizations or unique customers.

What is very interesting is that, even for the largest transformer taken into account (40 MVA), the simulated voltage dip at the energizing bus is not even close to critical levels if compared to the grid standards:

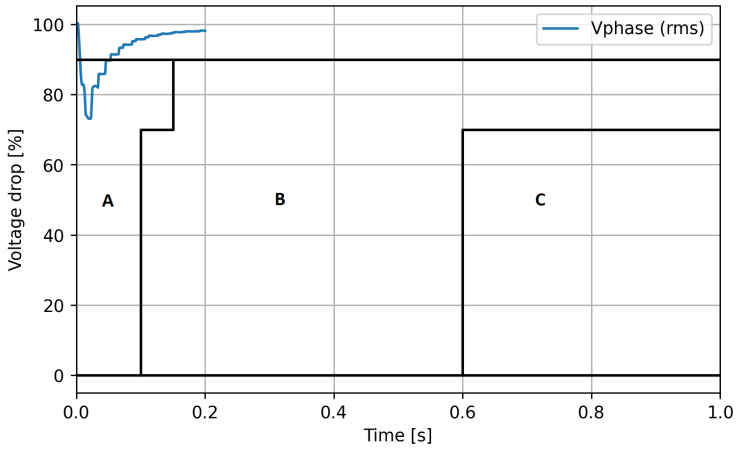

Figure 54: Voltage drop simulation (0.2s) of the hypothetical energization of a 40 MVA transformer in the Öland area, compared to the grid standards.

The short-circuit capacity of the energizing bus is 135 MVA, which means that the ratio of the transformer size (40 MVA) to the short-circuit capacity is almost 30%, three times more than the rule of thumb discussed in the introductory chapter. For this case, the recovery time is very short, and the magnitude is not extremely worrying, which leads us to an important conclusion: the rule of thumb that indicates a maximum transformer size of 10% with respect to the short-circuit capacity is very conservative, especially if we take into account that the chosen location of the grid from which the results were obtained corresponds to a weak bus in a remote island of Sweden.

This page is intentionally left blank

9 Conclusion

This MSc Thesis terminates with a summary of the achievements, possible improvements, conclusions, and future work that can potentially upgrade and verify the presented results.

The primary motivation of this MSc is to design a tool to aid in grid connection studies that focuses on the consequences of transformer energization. The original idea was that the tool automatically decides which is the largest transformer that can be installed on a particular bus without causing critical damage. However, the goals were gradually changed to interact more with the user and leave them responsible for deciding the transformer size boundary. One of the main reasons for these changes is the difficulties encountered in verifying the estimation of the energization impact on the surrounding network, for which site measurements could be of remarkable usefulness.

To estimate the effect of inrush currents in the surrounding network, it is first necessary to simulate the energization phenomenon appropriately. Substantial limitations involving technical complexity and available information remove the possibility of designing a detailed and precise transformer model. A simpler and generalized model based on a bank of single-phase transformers is constructed instead with surprising accuracy, especially considering the mathematical difficulties in solving the differential equations and the lack of specific references for such types of numerical problems.

This report focuses on the voltage dip produced due to the great current that flows from the system sources to the energized transformer because it is the main concern at E.ON. However, the typical measured voltage dips (Figure 47) and calculated values (even for larger transformers) are far from the danger zone according to Swedish regulations (Figures 40 and 41), which means that there might be strong consequences not being considered, the requirements are too lax, or the simplifications made during the model development are not precise enough. A good answer to this question could be to investigate historical data regarding unsatisfactory switching of transformers and their consequences. It has also been demonstrated that the rule of thumb that E.ON uses is not representative of all scenarios if we take into account only the RMS voltage drop and grid standards as the main reference.

In conclusion, taking into account the limitations and assumptions of the programmed tool, it is possible to have some intuition on the expected impact of energizing a transformer in the grid in terms of the voltage dip. However, some effort into verification is necessary.

9.1 Future Work

Finally, a list of suggested improvements is presented:

- Investigate in more detail the possibility of using unbalanced short circuit calculations as an additional possibility to analyse the voltage dip in the grid.
- Compare the results obtained in the grid analysis with a detailed dynamic model or measurements. This will help determine if any of the proposed strategies provide realistic solutions.
- Although inrush currents are usually damped in the range of a few seconds to minutes, it will be interesting to explore how tap changer transformers can fasten the voltage recovery.

- Analyse the effect of the Peterson Coil during the energization of a transformer.
- Design a model that can be used in three winding transformers.
- Add extra functionalities to the GUI.

References

[1] Jinsheng Peng et al. "Comparisons of normal and sympathetic inrush and their implications toward system voltage depression". In: *45th International Universities Power Engineering Conference UPEC2010*. 2010, pp. 1–5.

[2] Seyed Alireza Mousavi Mirkalaei and Fahd Hashiesh. "Controlled switching to mitigate power transformers inrush current phenomenon". In: *2015 50th International Universities Power Engineering Conference (UPEC)*. 2015, pp. 1–4. DOI: 10.1109/UPEC.2015.7339891.

[3] Shang Liqun et al. "Transformer Inrush Simulation And Analysis". In: *2019 IEEE 2nd International Conference on Electronics and Communication Engineering (ICECE)*. 2019, pp. 369–372. DOI: 10.1109/ICECE48499.2019.9058576.

[4] Thanh Bao Doan and Chi Phi Do. "Calculation of the Magnetic Field and Inrush Current in a Three-phase Transformer". In: *2020 Applying New Technology in Green Buildings (ATiGB)*. 2021, pp. 94–99. DOI: 10.1109/ATiGB50996.2021.9423111.

[5] Conseil international des grands réseaux électriques. Comité d'études C4. *Transformer Energization in Power Systems: A Study Guide*. CIGRÉ, 2014. ISBN: 9782858732630.

[6] Ning Chen et al. "The inrush current analysis and restraining method of energizing no-load transformer". In: *2016 3rd International Conference on Systems and Informatics (ICSAI)*. 2016, pp. 204–207. DOI: 10.1109/ICSAI.2016.7810955.

[7] Maria Cristina Nițu et al. "Ensuring the security of the energy system by predetermining the size of inrush current at power transformers coupling". In: *IEEE EUROCON 2015 - International Conference on Computer as a Tool (EUROCON)*. 2015, pp. 1–4. DOI: 10.1109/EUROCON.2015.7313772.

[8] H. C. Seo and C. H. Kim. "The analysis of power quality effects from the transformer inrush current: A case study of the Jeju power system, Korea". In: *2008 IEEE Power and Energy Society General Meeting - Conversion and Delivery of Electrical Energy in the 21st Century*. 2008, pp. 1–6. DOI: 10.1109/PES.2008.4596173.

[9] A. Pors and N. Browne. "Modelling the energisation of a generator step-up transformer from the high voltage network". In: *2008 Australasian Universities Power Engineering Conference*. 2008, pp. 1–5.

[10] MIT Department of Electrical Engineering. "The Magnetic-Circuit Concept". In: *Magnetic Circuits and Transformers: A First Course for Power and Communication Engineers*. 1977, pp. 41–53.

[11] E. Styvaktakis and M.H.J. Bollen. "Signatures of voltage dips: transformer saturation and multistage dips". In: *IEEE Transactions on Power Delivery* 18.1 (2003), pp. 265–270. DOI: 10.1109/TPWRD.2002.804016.

[12] W.L.A. Neves and H.W. Dommel. "On modelling iron core nonlinearities". In: *IEEE Transactions on Power Systems* 8.2 (1993), pp. 417–425. DOI: 10.1109/59.260845.

[13] L.F. Blume. *Transformer Engineering*. General Electric series. John Wiley & Sons Canada, Limited, 1951. ISBN: 9780471083498.

[14] MIT Department of Electrical Engineering. "Alternating-Current Excitation Characteristics of Iron-Core Reactors and Transformers". In: *Magnetic Circuits and Transformers: A First Course for Power and Communication Engineers*. 1977, pp. 156–211.

[15] Juan A. Martinez-Velasco and Ferley Castro-Aranda. *Transient Analysis of Power Systems - A Practical Approach*. John Wiley & Sons, Ltd, 2020. ISBN: 9781119480549. DOI: https://doi.org/10.1002/9781119480549.ch6.

[16] Hans Høidalen et al. "Developments in the hybrid transformer model – Core modeling and optimization". In: 2011.

[17] Nicola. Chiesa. *Power Transformer Modeling for Inrush Current Calculation*. https://ntnuopen.ntnu.no/ntnu-xmlui/handle/11250/256440. Accessed: 2022-05-29.

[18] Lars Eivind Jensvoll. "Transients During Energization of Unloaded Generator Step-Up Transformers". In: June 2019.

[19] Francisco de Leon, Ashkan Farazmand, and Pekir Joseph. "Comparing the T and π Equivalent Circuits for the Calculation of Transformer Inrush Currents". In: *IEEE Transactions on Power Delivery* 27.4 (2012), pp. 2390–2398. DOI: 10.1109/TPWRD.2012.2208229.

[20] Majid Salimi, Aniruddha Gole, and Rohitha P. Jayasinghe. "Improvement of Transformer Saturation Modeling for Electromagnetic Transient Programs". In: 2013.

[21] *The Classical Approach –PSCAD –*. https://www.pscad.com/webhelp/EMTDC/Transformers/The_Classical_Approach/the_classical_approach.htm. Accessed: 2022-05-25.

[22] A. Ametani. *Numerical Analysis of Power System Transients and Dynamics*. Jan. 2015, pp. 1–531. ISBN: 9781849198493. DOI: 10.1049/PBPO078E.

[23] Endre Süli and David F. Mayers. *An Introduction to Numerical Analysis*. University of Iowa, 2003. DOI: 10.1017/CBO9780511801181.

[24] *Trapezoidal Method*. https://www.scribd.com/document/239258647/Numerical-Solution-RL-Circuit. Accessed: 2022-05-26.

[25] Juan de la Peña Toledo. *Python algorithm to simulate the energization of three-phase transformers*. https://github.com/juano-98/TransformerEnergization.git.

[26] C. Carrillo et al. "Analysis of the transformer inrush current in a hydro generator". In: *2016 IEEE 16th International Conference on Environment and Electrical Engineering (EEEIC)*. 2016, pp. 1–6. DOI: 10.1109/EEEIC.2016.7555576.

[27] K. Shaarbafi. "Transformer Modelling Guide - AESO". In: 2014.

[28] Arthur Ekwue and Barry Rawn. "Investigations into the transformer inrush current problem". In: *Nigerian Journal of Technology* 37 (Nov. 2018), p. 1058. DOI: 10.4314/njt.v37i4.27.

[29] *Application Program Interface (API) PSS®E 35.3.0*.

[30] Jinsheng Peng. "Assessment of Transformer Energisation Transients and Their Impacts on Power Systems". In: *PhD thesis submitted to the University of Manchester* (Aug. 2014).

[31] Charles R. Harris et al. "Array programming with NumPy". In: *Nature* 585 (2020), pp. 357–362. DOI: 10.1038/s41586-020-2649-2.

[32] *Föreskrift EIFS 2013:1 – Energimarknadsinspektionens föreskrifter och allmänna råd om krav som ska vara uppfyllda för att överföringen av el ska vara av god kvalitet EIFS 2013:1*. https://www.ei.se/om-oss/publikationer/publikationer/foreskrifter-el/2013/foreskrift-eifs-20131. Accessed: 2022-05-27.

[33] *Python interface to Tcl/Tk*. https://github.com/python/cpython/blob/3.10/Doc/library/tkinter.rst. Accessed: 2022-05-29.

Appendix

Appendix A: Influence of Residual Flux and Voltage Point in the Inrush Current for a Wye/Wye Transformer with Primary Directly Grounded

• Zero voltage crossing (phase A) and zero residual flux:

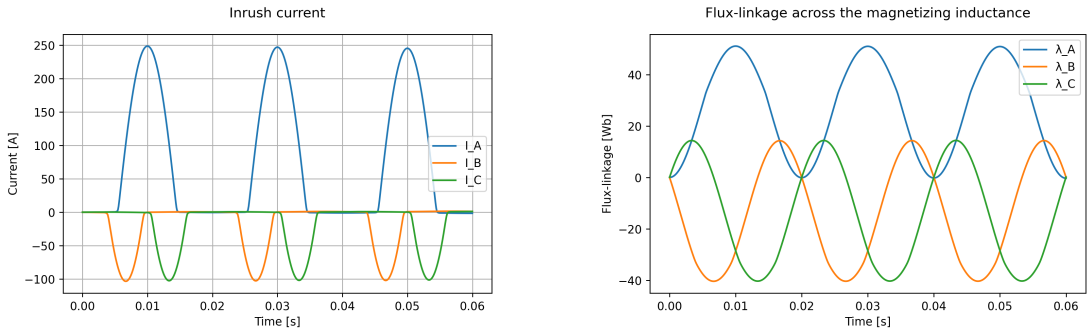

(a) **(b)**

Figure 55: Simulated current (a) and flux (b) during the energization of the transformer in Table 3 when connected in Wye/Wye and energized at zero voltage crossing and zero residual flux.

• Zero voltage crossing (phase A) and maximum residual flux:

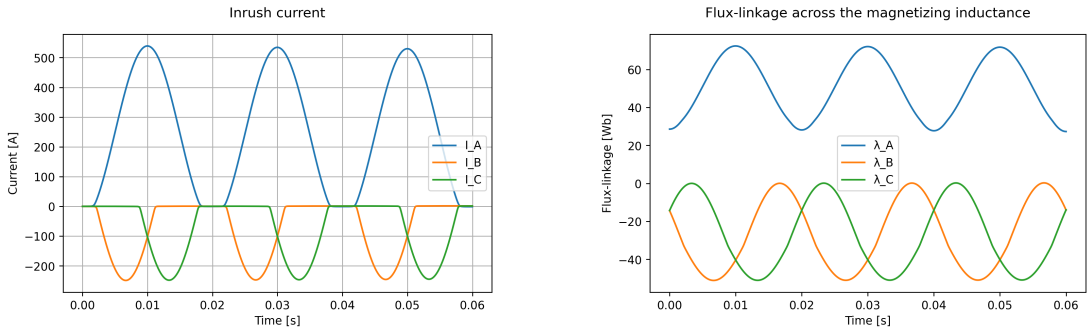

(a) **(b)**

Figure 56: Simulated current (a) and flux (b) during the energization of the transformer in Table 3 when connected in Wye/Wye and energized at zero voltage crossing and maximum residual flux.

• 45^{o} lagging voltage crossing (phase A) and zero residual flux:

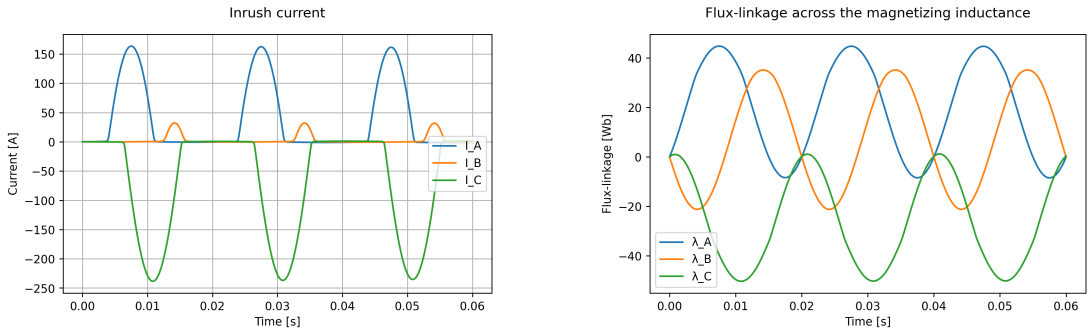

(a) **(b)**

Figure 57: Simulated current (a) and flux (b) during the energization of the transformer in Table 3 when connected in Wye/Wye and energized at 45^{o} voltage crossing and zero residual flux.

Appendix B: Code for Wye/Delta Transformer with Primary Directly Grounded

The following code is a reduced version of the original, which can be found in the Github repository [25]

Code starts in the next page.

```
# -*- coding: utf-8 -*-
"""
Created on April 6 2022
@author: Juan de la Peña

"""

# 3Ø. Wye/g-Delta connection
# Assumptions:
# 1. Symmetric conditions, except for Lm ~
# 2. R, L, Lm, Rm, and Znetowork should be indicated per phase
# 3. Neutral connected to ground
#
# ØA
#                      V_AN_bus
# V_AN --- Znetwork --- / --- R1 ----L1------------------> I_delta
#                                    |       |
#                                  Lm ~     Rm
#                                    |       |
#                                    N       N
#
# Internal voltages always refered to neutral: Vm_A => Vm of phase A refered to neutral
# V_AN_bus phase bus voltage
# V_AB_bus line bus voltage
#
# IMPORTANT --> VALID SCRIPT ONLY IF (L*Lm/Rm) IS SIGNIFICANTLY SMALL -->
# REDUCES ORDER OF DIFFERENTIAL EQUATION

import math
import numpy as np
from Saturation_curve_V2 import estimateInductance
from Saturation_curve_V2 import printSaturationCurve
import matplotlib.pyplot as plt

def EnergizationWyegDelta(V_L, V2_L, L1, L2, Lm, L_A, R1, R2, Rm, phi_0, f, flux_linkage_A_0, flux_linkage_B_0, flux_linkage_C_0, Rnetwork, Lnetwork, K, N, dt, t_stop, change_resolution, bus_energ_voltage_pu):
    """
    Function to perform the energization simulation of a Wye - Delta transformerm with primary winding grounded

    Winding 1 is energized, secondary is unloaded. Winding 1 should be the HV side, as it is energized from the grid.

    Description of INPUT parameters:
    V_L --> Line rated voltage of winding 1, in rms.
    V_2L --> Line rated voltage of winding 2, in rms. Converted AFTERWARDS to LINE for Wye and PHASE for Delta.
    L1 --> Leakage inductance winding 1, in H
    L2 --> Leakage inductance winding 2, in H
    Lm --> Unsaturated magnetizing inductance, with respect winding 1, in H
    L_A --> Saturated magnetizing inductance, with respect winding 1, in H
    R1 --> Winding 1 resistance, in ohm
    R2 --> Winding 2 resistance, in ohm
    Rm --> Magnetizing resistance, with respect winding 1, in ohm
    phi_0 --> Phase shift voltage source with respect to reference. Line voltage BC is at 0 degrees if no shift is applied.
    f --> Frequency, in Hz
    flux_linkage_A/B/C_0 --> Residual flux of each phase, in Wb
    Rnetwork & Lnetwork --> Equivalent resistance and inductance of connecting bus
    K --> Knee point, in pu
    N --> Number of points for linearization of saturation curve. 10 is recommended.
    dt --> Time step size, in s. 5*10**-6 is recommended.
    t_stop --> Simulation time, in s. Recommended up to 0.2 - 0.5 s
    bus_energ_voltage_pu --> Voltage in pu of energizing bus

    """

    # Calculate angular speed
    w = 2*math.pi*f

    # Include Rnetwork and Lnetwork inside R and L, as this will not affect the inrush current calculation methodology
    R = R1 + Rnetwork
    L = L1 + Lnetwork

    # Create variables for three phase system
    V_F = V_L/math.sqrt(3) #V #tension de fase rms
    V_L_max = V_L*math.sqrt(2) #V #tension de linea pico
    V_F_max = V_F*math.sqrt(2) #V #tension de fase pico

    # Secondary resistance and inductance refered to the first winding
    L21 = 3*L2*(V_F/V2_L)**2 #Leakage reactance of secondary winding referred to first winding: it should have the same value as L1
    R21 = 3*R2*(V_F/V2_L)**2 #Winding resistance of secondary winding referred to first winding: it should have the same value as R1

    #Initialization
    Il_A = 0 #initial conditions
    Il_B = 0 #initial conditions
    Il_C = 0 #initial conditions
    I_A = 0 #initial conditions
    I_B = 0 #initial conditions
    I_C = 0 #initial conditions
    I_delta = 0 #initial conditions
    t = 0 #initial value
    flux_linkage_A = flux_linkage_A_0 #initial value
    flux_linkage_B = flux_linkage_B_0 #initial value
    flux_linkage_C = flux_linkage_C_0 #initial value
    V_AB_bus_rms = V_L #initial value
    V_AN_bus_rms = V_F #initial value
    V_BC_bus_rms = V_L #initial value
    V_BN_bus_rms = V_F #initial value
    V_CA_bus_rms = V_L #initial value
    V_CN_bus_rms = V_F #initial value
    I_A_rms = 0 #initial value
    I_B_rms = 0 #initial value
    I_C_rms = 0 #initial value

    #trapezoidal variables
    flux_linkage_sum_prev = 0
    I_delta_prev = I_delta
    I_delta_prev_prev = I_delta_prev
    Il_A_prev = 0
    V_AN_prev = V_F_max*math.sin(phi_0 + 90*2*math.pi/360)*bus_energ_voltage_pu
    flux_linkage_A_prev = flux_linkage_A_0 #initial value
    Il_B_prev = 0
    V_BN_prev = V_F_max*math.sin(phi_0 - 30*2*math.pi/360)*bus_energ_voltage_pu
    flux_linkage_B_prev = flux_linkage_B_0 #initial value
    Il_C_prev = 0
    V_CN_prev = V_F_max*math.sin(phi_0 - 150*2*math.pi/360)*bus_energ_voltage_pu
    flux_linkage_C_prev = flux_linkage_C_0 #initial value

    while t <= t_stop:

        #LINE VOLTAGES
        V_AB = V_L_max*math.sin(w*t + phi_0 + 120*2*math.pi/360)*bus_energ_voltage_pu #line voltage A-B --> + 120º
        V_BC = V_L_max*math.sin(w*t + phi_0)*bus_energ_voltage_pu #line voltage B-C --> 0º
        V_CA = V_L_max*math.sin(w*t + phi_0 - 120*2*math.pi/360)*bus_energ_voltage_pu #line voltage C-A --> - 120º

        #PHASE VOLTAGES
        V_AN = V_F_max*math.sin(w*t + phi_0 + 90*2*math.pi/360)*bus_energ_voltage_pu #phase voltage A-N --> + 90º
        V_BN = V_F_max*math.sin(w*t + phi_0 - 30*2*math.pi/360)*bus_energ_voltage_pu #phase voltage B-N --> - 30º
        V_CN = V_F_max*math.sin(w*t + phi_0 - 150*2*math.pi/360)*bus_energ_voltage_pu #phase voltage C-N --> - 150º

        #calculate variable magnetizing inductance
        Lm_A_variable = estimateInductance(V_F, Lm, L_A, f, K, N, abs(flux_linkage_A)) #don't need to introduce the abs value as this is already done in the function
        Lm_B_variable = estimateInductance(V_F, Lm, L_A, f, K, N, abs(flux_linkage_B))
        Lm_C_variable = estimateInductance(V_F, Lm, L_A, f, K, N, abs(flux_linkage_C))

        #---- FIRST ESTIMATES ----
        #main ØA
        B_A = Lm_A_variable*R/Rm + L + Lm_A_variable
        Il_A = 1/(1+dt/2*R/B_A)*(Il_A_prev + dt/2*((V_AN_prev - I_delta_prev*R - (I_delta_prev - I_delta_prev_prev)/dt*L)/B_A - Il_A_prev*R/B_A + (V_AN - I_delta*R - (I_delta - I_delta_prev)/dt*L)/B_A))
        I_A = Il_A + Lm_A_variable/Rm*(Il_A - Il_A_prev)/dt + I_delta
        flux_linkage_A = flux_linkage_A_prev + Lm_A_variable*(Il_A - Il_A_prev)

        #main ØB
        B_B = Lm_B_variable*R/Rm + L + Lm_B_variable
        Il_B = 1/(1+dt/2*R/B_B)*(Il_B_prev + dt/2*((V_BN_prev - I_delta_prev*R - (I_delta_prev - I_delta_prev_prev)/dt*L)/B_B - Il_B_prev*R/B_B + (V_BN - I_delta*R - (I_delta - I_delta_prev)/dt*L)/B_B))
        I_B = Il_B + Lm_B_variable/Rm*(Il_B - Il_B_prev)/dt + I_delta
        flux_linkage_B = flux_linkage_B_prev + Lm_B_variable*(Il_B - Il_B_prev)

        #main ØC
        B_C = Lm_C_variable*R/Rm + L + Lm_C_variable
        Il_C = 1/(1+dt/2*R/B_C)*(Il_C_prev + dt/2*((V_CN_prev - I_delta_prev*R - (I_delta_prev - I_delta_prev_prev)/dt*L)/B_C - Il_C_prev*R/B_C + (V_CN - I_delta*R - (I_delta - I_delta_prev)/dt*L)/B_C))
        I_C = Il_C + Lm_C_variable/Rm*(Il_C - Il_C_prev)/dt + I_delta
        flux_linkage_C = flux_linkage_C_prev + Lm_C_variable*(Il_C - Il_C_prev)

        #delta current
        flux_linkage_sum = flux_linkage_A + flux_linkage_B + flux_linkage_C
        I_delta_prev_prev = I_delta_prev
        I_delta_prev = I_delta
        I_delta = ((flux_linkage_sum - flux_linkage_sum_prev - 3*(R21*dt/2-L21)*I_delta_prev)/(3*(R21*dt/2+L21)))
        #---- FIRST ESTIMATES ----
```

```
#---- NEWTON ITERATIVE METHOD ----
tolerance_value = 1*10**-5
tolerance = np.array([[tolerance_value],
                      [tolerance_value],
                      [tolerance_value],
                      [tolerance_value]])
estimate = np.array([[I1_A], [I1_B], [I1_C], [I_delta]])
solution = np.array([[999999], [999999], [999999], [999999]]) #choose any random improbable value
while np.all(abs(solution - estimate) > tolerance):
    function = np.array([[I1_A - 1/(1+dt/2*R/B_A)*(I1_A_prev + dt/2*((V_AN_prev - I_delta_prev*R - (I_delta_prev - I_delta_prev_prev)/dt*L)/B_A - I1_A_prev*R/B_A + (V_AN - I_delta*R - (I_delta - I_delta_prev)/dt*L)/B_A))],
                         [I1_B - 1/(1+dt/2*R/B_B)*(I1_B_prev + dt/2*((V_BN_prev - I_delta_prev*R - (I_delta_prev - I_delta_prev_prev)/dt*L)/B_B - I1_B_prev*R/B_B + (V_BN - I_delta*R - (I_delta - I_delta_prev)/dt*L)/B_B))],
                         [I1_C - 1/(1+dt/2*R/B_C)*(I1_C_prev + dt/2*((V_CN_prev - I_delta_prev*R - (I_delta_prev - I_delta_prev_prev)/dt*L)/B_C - I1_C_prev*R/B_C + (V_CN - I_delta*R - (I_delta - I_delta_prev)/dt*L)/B_C))],
                         [I_delta - ((flux_linkage_sum - flux_linkage_sum_prev - 3*(R21*dt/2-L21)*I_delta_prev)/(3*(R21*dt/2+L21)))]])

    #Jacobian matrix
    J = np.array([[1, 0, 0, -1/(1+dt/2*R/B_A)*dt/2*(1/B_A*(-R-L/dt))],
                  [0, 1, 0, -1/(1+dt/2*R/B_B)*dt/2*(1/B_B*(-R-L/dt))],
                  [0, 0, 1, -1/(1+dt/2*R/B_C)*dt/2*(1/B_C*(-R-L/dt))],
                  [-Lm_A_variable/(3*(R21*dt/2+L21)), -Lm_B_variable/(3*(R21*dt/2+L21)), -Lm_C_variable/(3*(R21*dt/2+L21)), 1]])

    if solution[0, 0] != 999999:
        estimate = solution.copy()
    solution = estimate - np.matmul(np.linalg.inv(J),function)
    I_delta = solution[3, 0]
    I1_A = solution[0, 0]
    I1_B = solution[1, 0]
    I1_C = solution[2, 0]
    I_A = I1_A + Lm_A_variable/Rm*(I1_A - I1_A_prev)/dt + I_delta
    flux_linkage_A = flux_linkage_A_prev + Lm_A_variable*(I1_A - I1_A_prev)
    I_B = I1_B + Lm_B_variable/Rm*(I1_B - I1_B_prev)/dt + I_delta
    flux_linkage_B = flux_linkage_B_prev + Lm_B_variable*(I1_B - I1_B_prev)
    I_C = I1_C + Lm_C_variable/Rm*(I1_C - I1_C_prev)/dt + I_delta
    flux_linkage_C = flux_linkage_C_prev + Lm_C_variable*(I1_C - I1_C_prev)
    flux_linkage_sum = flux_linkage_A + flux_linkage_B + flux_linkage_C
#---- NEWTON ITERATIVE METHOD ----

#voltages
Vm_A = Lm_A_variable*(I1_A - I1_A_prev)/dt
Vm_B = Lm_B_variable*(I1_B - I1_B_prev)/dt
Vm_C = Lm_C_variable*(I1_C - I1_C_prev)/dt
# @A bus voltage
V_AN_bus = V_AN - I_A*Rnetwork - (V_AN-I_A*R-Vm_A)/L*Lnetwork
V_BN_bus = V_BN - I_B*Rnetwork - (V_BN-I_B*R-Vm_B)/L*Lnetwork
# @B bus voltage
V_BN_bus = V_BN - I_B*Rnetwork - (V_BN-I_B*R-Vm_B)/L*Lnetwork
V_CN_bus = V_CN - I_C*Rnetwork - (V_CN-I_C*R-Vm_C)/L*Lnetwork
# @C bus voltage
V_CN_bus = V_CN - I_C*Rnetwork - (V_CN-I_C*R-Vm_C)/L*Lnetwork
V_AN_bus = V_AN - I_A*Rnetwork - (V_AN-I_A*R-Vm_A)/L*Lnetwork

#trapezoidal variables
flux_linkage_sum_prev = flux_linkage_sum
I1_A_prev =  I1_A
V_AN_prev = V_AN
flux_linkage_A_prev = flux_linkage_A
I1_B_prev =  I1_B
V_BN_prev = V_BN
flux_linkage_B_prev = flux_linkage_B
I1_C_prev =  I1_C
V_CN_prev = V_CN
flux_linkage_C_prev = flux_linkage_C

t = t + dt #update time
```

Appendix C: Transformer Data Conversion

A typical transformer report provides data related to the short circuit and open circuit test. From these experiments is obtained the load losses P_{LL} (sometimes called copper losses) and leakage reactance, and the no load losses P_{NL} and magnetizing current $I_{exc}\%$ respectively. Together with the transformer rating information is enough to calculate the values of each element in the models described in Chapter 5.

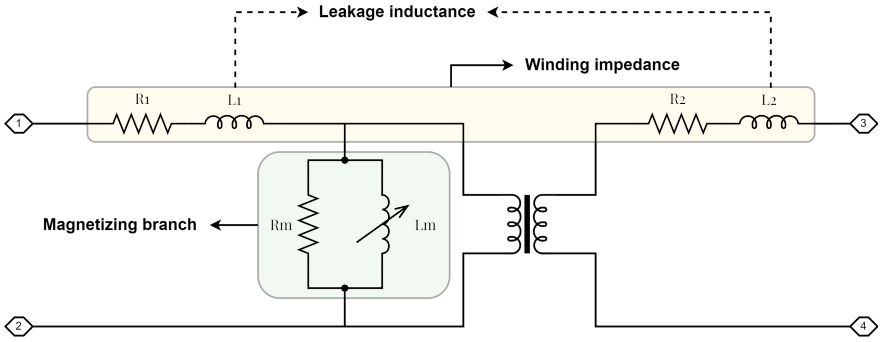

Figure 58: Nomenclature clarification (single-phase)

$$\text{Winding resistance } R(p.u.) = \frac{P_{LL}}{S_{rated}} \tag{51}$$

$$\text{Magnetizing branch admittance } Y(p.u.) = \frac{I_{exc}\%}{100} \tag{52}$$

$$\text{Magnetizing branch conductance } G(p.u.) = \frac{P_{NL}}{S_{rated}} \tag{53}$$

$$\text{Magnetizing branch susceptance } B(p.u.) = -\sqrt{Y^2 - G^2} \tag{54}$$

Where S_{rated} refers to the transformer rated power, providing that the test reports have been done at that exact value.

With Equations 51, 52, 53, 54, the leakage reactance, rated voltages and power, and connection type for the secondary winding it can be obtained R_1, L_1, R_2, L_2, L_M and R_m.

Notes: sometimes the winding impedance magnitude is given instead of the leakage reactance.